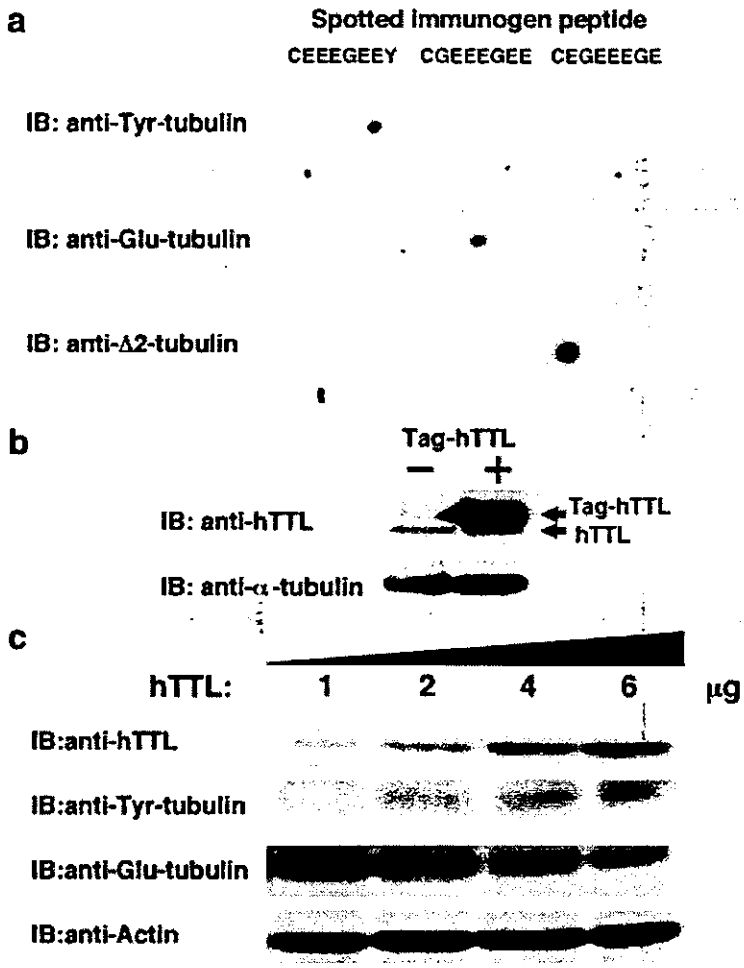

FIGURE 3 – hTTL has a tyrosination activity in mammalian cultured cells. (*a*) Specificity of antibodies. The indicated synthetic peptides were spotted on the filter and immunoblotted with the polyclonal anti-Tyr-tubulin (top), anti-Glu-tubulin (middle), or anti-Δ2-tubulin antibody (bottom). (*b*) Expression of FLAG-tagged hTTL. Whole-cell lysates prepared from COS7 cells transfected with the empty plasmid or with the expression plasmid for FLAG-tagged hTTL were subjected to immunoblotting with the anti-hTTL antibody (top). The expression level of α-tubulin was examined to ensure equal loading (bottom). (*c*) The exogenously expressed hTTL has a catalytic activity. HEK293T cells were transfected with increasing amounts of the hTTL expression plasmid. Forty-eight hours after transfection, whole-cell lysates were prepared and immunoblotted with the indicated antibodies. The expression level of actin is included as a loading control (bottom).

cells with 1 nM BMP2 or 5 μM RA induced remarkable morphologic differentiation by day 8. The hTTL protein level was increased after day 2 and peaked on day 6 in the former and on day 3 in the latter. Thereafter, it appeared to be decreased. Thus, hTTL was induced during induction of neuronal differentiation in NBL cells.

Expression of hTTL mRNA in primary neuroblastomas

To evaluate the clinical significance of *hTTL*, we examined the expression of *hTTL* mRNA in 16 favorable (stage 1, high expression of *TrkA* and a single copy of *MYCN*) and 16 unfavorable (stage 3 or 4, low expression of *TrkA* and amplification of *MYCN*) NBLs using semiquantitative RT-PCR. As shown in Figure 5(*a*), *hTTL* was preferentially expressed in favorable NBLs. Therefore, we next performed quantitative real-time RT-PCR to measure the levels of *hTTL* transcript in 74 primary NBLs. Table I shows the quantitative levels of *hTTL* mRNA expression (mean ± SEM) by age (< 1-year-old *vs.* ≥ 1-year-old), tumor stages (1 + 2 + 4s *vs.* 3 + 4), *TrkA* expression (low *vs.* high), *MYCN* gene copies (single *vs.* amplified), origin (adrenal gland *vs.* others), mass screening (tumors found by mass screening *vs.* sporadic tumors) and prognosis (alive *vs.* dead). High levels of *hTTL* expression were significantly associated with favorable stages ($p = 0.0069$), high *TrkA* expression ($p = 0.002$), a single copy of *MYCN* ($p < 0.00005$), tumors found by mass screening ($p = 0.0042$), origins other than adrenal gland ($p = 0.0042$) and a good prognosis ($p = 0.023$). *hTTL* expression was marginally associated with age. The log-rank test indicated that *hTTL* expression was associated with better survival ($p = 0.026$), which was also indicated in the Kaplan-Meier cumulative survival curves (Fig. 5*b*).

The univariate Cox regression was employed to examine the individual relationship of each variable to survival (Table II). Expression of *hTTL*, age, *MYCN* copy numbers and mass screening were found to be of prognostic importance, supporting the results of the log-rank test. However, since *hTTL* expression was highly associated with *MYCN*, mass screening and origin, multivariable Cox models were not fitted to assess the predictive importance of *hTTL* expression for survival after controlling these prognostic factors, suggesting that expression of *hTTL* was not an independent prognostic indicator.

FIGURE 2 – Genomic structure, alignment of amino acid sequence and mRNA expression of human *TTL*. (*a*) Genomic structure of *hTTL*. The *hTTL* gene that is mapped to 2q13 consists of 7 exons. Untranslated regions (open boxes) and coding regions (hatched boxes) are shown. Numbers indicate nucleotide position in human BAC clone *RP11-1124* (accession number AC012442). (*b*) Comparison of amino acid sequences among mammalian TTLs. The gaps produced by the alignment are indicated by a hyphen in the sequence. The conserved amino acid residues in TTLs are shown by asterisks below the alignment. (*c*) Tissue distribution of *hTTL* mRNA. The expression levels of *hTTL* mRNA in the indicated human tissues were examined by semiquantitative RT-PCR (top). *GAPDH* expression was also examined as an internal control (bottom).

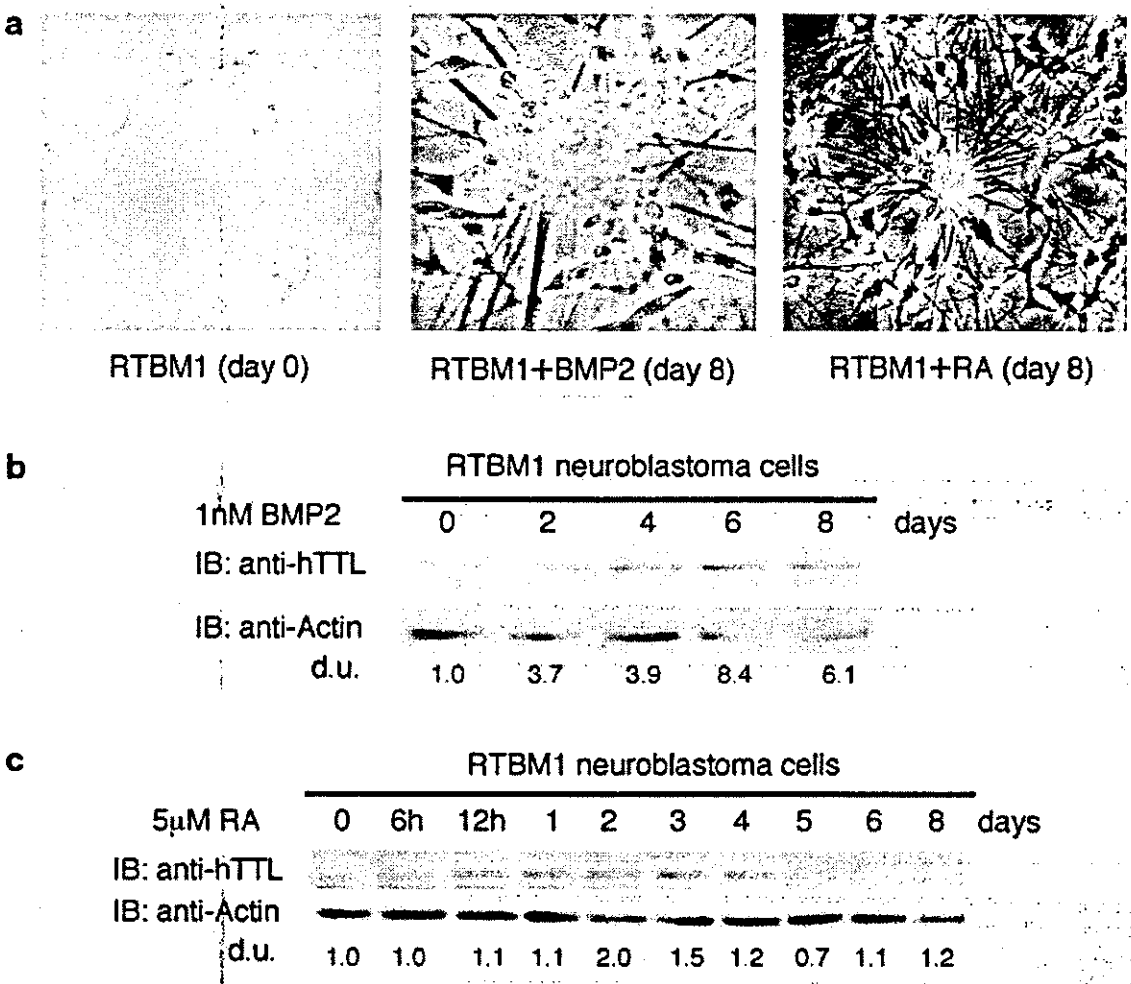

FIGURE 4 – TTL is induced during BMP2- and RA-mediated neuroblastoma differentiation. (*a*) BMP2- or RA-induced morphologic changes in RTBM1 neuroblastoma cells. RTBM1 cells were treated with BMP2 or RA at a final concentration of 1 nM or 5 μM, respectively, and maintained for 8 days. (*b*) Expression levels of hTTL are increased in response to BMP2. At the indicated time points after the treatment with BMP2 (at a final concentration of 1 nM), whole-cell lysates prepared from RTBM1 cells were subjected to immunoblotting with the antibody against hTTL (top). Actin protein levels were determined as a loading control (bottom). (*c*) Induction of hTTL in response to RA. RTBM1 cells were exposed to RA at a final concentration of 5 μM. Whole-cell lysates were prepared at the indicated time points after the treatment with RA and subjected to immunoblotting with the anti-hTTL (top) or with antiactin (bottom) antibody. d.u., arbitrary density units.

Immunohistochemistry

To determine the expression pattern of hTTL protein in primary NBLs, we performed immunohistochemical study for 6 favorable (stage 1 or 2 and a single copy of *MYCN*) and 4 unfavorable (stage 3 or 4 and amplified *MYCN*) NBLs. hTTL, Tyr-tubulin and Glu-tubulin were positively detected both in the cytoplasm of the neuroblastic cells and in the fine meshwork of neuropil of all 6 tumors with favorable histology (Shimada's classification) and a single copy of *MYCN* (Fig. 6*a–c*). In contrast, all 4 tumors with unfavorable histology and *MYCN* amplification were negative for Tyr-tubulin and Glu-tubulin, and only 1 tumor in this subset was positive for hTTL (Fig. 6*f–h*). Interestingly, all 10 NBL tumors were positive for Δ2-tubulin, but whose staining pattern was rather distinct in different subsets of the tumors. In the favorable tumors, Δ2-tubulin showed a localization similar to hTTL, Tyr-tubulin and Glu-tubulin and was detected in the cytoplasm and in the fine neuropil (Fig. 6*d*). On the other hand, Δ2-tubulin in the aggressive tumors was found only in the cytoplasm of neuroblastic cells, since they had no or a very limited capability of neuritic process production (*i.e.*, neuropil formation; Fig. 6*i*).

CD56 was detected in all 10 tumors, regardless of the histology and *MYCN* status (data not shown). TrkA was detected in all of 6 favorable tumors (Fig. 6*e*), but was negative in 3 of 4 aggressive tumors (Fig. 6*j*). It was noted that one unfavorable tumor with weakly positive trkA showed positive staining for TTL. Ki-67 staining revealed 10–20% and 60–70% positive cells in the favorable and the unfavorable tumors, respectively (data not shown).

DISCUSSION

In the present study, we have identified human ortholog of *tubulin tyrosine ligase* gene, which is highly conserved among the mammalian species. *hTTL* mRNA is ubiquitously expressed but rather preferential in both fetal and adult brains as well as in lung. The specific antibodies raised against hTTL, Tyr-tubulin, Glu-tubulin and Δ2-tubulin have confirmed the catalytic activity of

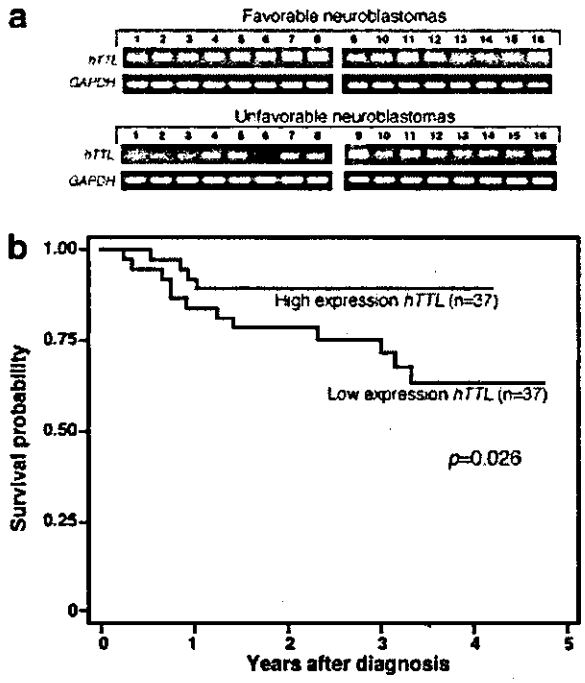

FIGURE 5 – Expression of *hTTL* mRNA is associated with unfavorable prognosis of neuroblastoma. (*a*) Total RNA was purified from the indicated favorable (top) and unfavorable NBL tissues (bottom) and subjected to semiquantitative RT-PCR. Sixteen favorable cases used in this study were classified as stage 1 NBL with a single copy *MYCN* as well as a high expression of *TrkA*. Sixteen unfavorable cases were in stages 3 and 4 NBL with *MYCN* amplification as well as a low *TrkA* expression. *GAPDH* expression was also examined as an internal control. (*b*) Association of *hTTL* mRNA expression levels with favorable prognosis of NBL. Total RNA was prepared from 74 NBL tissues, and *hTTL* mRNA levels were assayed by quantitative real-time RT-PCR as described in text. The values of *hTTL* mRNA were normalized by *GAPDH*. The survival of *hTTL* relatively high-expression group (n = 37) and *hTTL* low-expression group (n = 37) was compared using the Kaplan-Meier procedure.

TABLE I – RESULTS OF LOG-RANK TESTS FOR CONVENTIONAL PROGNOSTIC FACTORS AND EXPRESSION OF *hTTL* IN 74 PRIMARY NEUROBLASTOMAS

Variable	n	*hTTL* expression[1]	p-value
Age (year)			0.1
<1	43	117 ± 14	
≥1	31	77 ± 10	
Tumor stage			0.0069
1, 2, 4s	40	127 ± 14	
3, 4	34	69 ± 9	
TrkA expression			0.002
High	36	125 ± 17	
Low	38	77 ± 8	
MYCN			<0.00005
Single	52	123 ± 11	
Amplified	22	46 ± 9	
Mass screening			0.0042
+	37	128 ± 14	
−	37	72 ± 10	
Origin			0.0042
Adrenal gland	47	85 ± 11	
Others	27	127 ± 16	
Prognosis			0.023
Alive	58	113 ± 11	
Dead	16	54 ± 11	

[1]Mean ± SEM.

TABLE II – COX REGRESSION MODELS USING DICHOTOMOUS FACTORS OF AGE, *MYCN* AMPLIFICATION, MASS SCREENING, ORIGIN AND EXPRESSION OF *hTTL*

Factor	p-value	Hazard ratio (95% confidence interval)
hTTL expression (log)	0.024	0.64 (0.44, 0.94)
Age (> 1 *vs.* < 1 year)	0.005	5.04 (1.61, 15.8)
MYCN (1 copy *vs.* > 1 copy)	<0.0005	0.06 (0.017, 0.22)
Mass screening (+ *vs.* −)	0.004	0.05 (0.007, 0.38)
Origin (adrenal gland *vs.* others)	0.31	1.79 (0.58, 5.57)

hTTL encoded by the *hTTL* gene in the cells. Interestingly, hTTL is induced during neurite extension in RTBM1 NBL cells treated with BMP2 or RA, suggesting that hTTL expression is associated with neuronal differentiation in human NBL. Immunohistochemically, favorable NBLs are positive for hTTL, Tyr-tubulin, Glu-tubulin and Δ2-tubulin, whereas unfavorable tumors with *MYCN* amplification are positive only for Δ2-tubulin, suggesting that deregulation of tyrosination/detyrosination cycle contributes to malignant progression of NBL. This hypothesis has been further supported by a significant decrease of the levels of *hTTL* expression in the patients with poor prognosis.

The dynamics of microtubule regulates many cellular functions, including migration, motility, differentiation, cell division and cellular cap formation. Though posttranslational modifications of tubulin and their enzymatic regulation have long been studied, the precise mechanisms are still largely unknown. It is interesting that no orthologs of highly conserved mammalian TTL have so far been reported in *Caenorhabditis elegans*, *Drosophila melanogaster* and *Saccharomyces cerevisiae*, suggesting that the tyrosination/detyrosination cycle of tubulin may be related to evolution of the cellular functions, including neuronal differentiation. In newborn rats, TTL expression is found in skeletal muscle at high levels and is developmentally regulated by rapidly decreasing its level during early postnatal period.[31] It is interesting that both BMP2 and RA, which have increased levels of hTTL expression, function as regulators to induce differentiation during neural development.

The tyrosination/detyrosination of tubulin may be regulated by the activities of both TTL and tubulin carboxypeptidase (TCP). Until now, however, the *TCP* gene has never been identified in vertebrates, although biochemical TCP activity has been reported to be present in some subcellular fractions.[18] Tubulin is also posttranslationally modified by nitrotyrosination. Eiserich *et al.*[32] showed that free 3-nitrotyrosine (NO_2Tyr) is transported into mammalian cells and selectively incorporated into the Glu-tubulin posttranslationally, which is catalyzed by TTL. Cellular injury such as microtubule disorganization has consequently been induced. Kalisz *et al.*[33] also showed that nitrotyrosine can be incorporated into α-tubulin by *in vitro* assays. Those reports demonstrated that carboxypeptidase A is incapable of cleaving nitrotyrosine from the modified α-tubulin. On the other hand, Bisig *et al.*[34] reported that nitrotyrosinated tubulin is a good substrate of physiologic TCP, and that it has a similar capability to that of the tyrosinated tubulin to assemble into microtubules, suggesting that incorporation of nitrotyrosine is not injurious at least to dividing cells. Therefore, whether nitrotyrosinated tubulin is harmful or not is still controversial. Nevertheless, as increased nitrotyrosination is reported in Alzheimer's disease and amyotrophic lateral sclerosis,[35–37] the functional analysis of the role of hTTL and tubulin tyrosination/detyrosination cycle should be important for understanding the pathogenesis of these disease. The treatment of cells with methylmercury (MeHg) is also reported to induce perturbation of cellular activities associated with the tubulin/microtubule system by altering the status of tubulin tyrosination in the rat

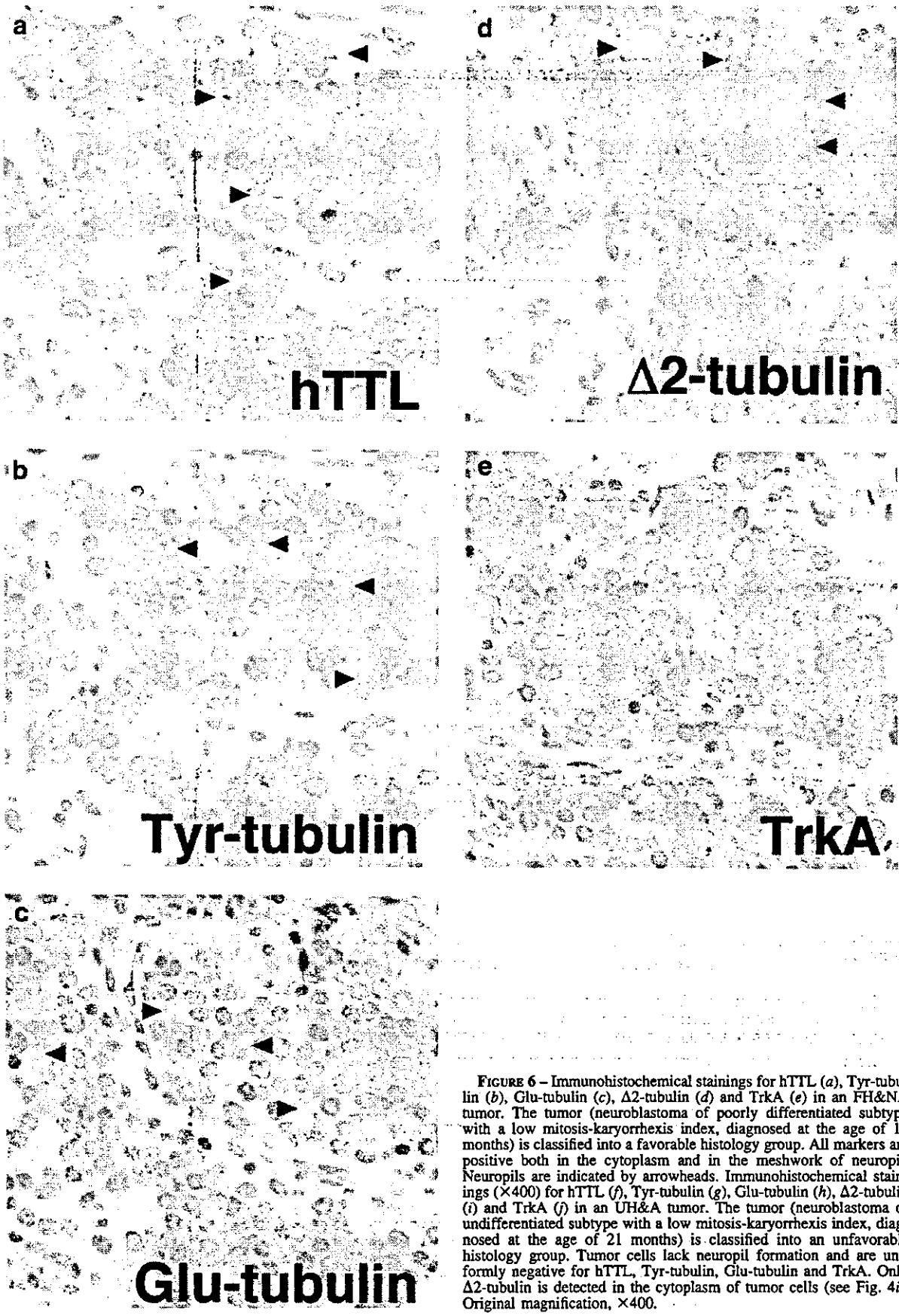

FIGURE 6 – Immunohistochemical stainings for hTTL (*a*), Tyr-tubulin (*b*), Glu-tubulin (*c*), Δ2-tubulin (*d*) and TrkA (*e*) in an FH&NA tumor. The tumor (neuroblastoma of poorly differentiated subtype with a low mitosis-karyorrhexis index, diagnosed at the age of 10 months) is classified into a favorable histology group. All markers are positive both in the cytoplasm and in the meshwork of neuropil. Neuropils are indicated by arrowheads. Immunohistochemical stainings (×400) for hTTL (*f*), Tyr-tubulin (*g*), Glu-tubulin (*h*), Δ2-tubulin (*i*) and TrkA (*j*) in an UH&A tumor. The tumor (neuroblastoma of undifferentiated subtype with a low mitosis-karyorrhexis index, diagnosed at the age of 21 months) is classified into an unfavorable histology group. Tumor cells lack neuropil formation and are uniformly negative for hTTL, Tyr-tubulin, Glu-tubulin and TrkA. Only Δ2-tubulin is detected in the cytoplasm of tumor cells (see Fig. 4*i*). Original magnification, ×400.

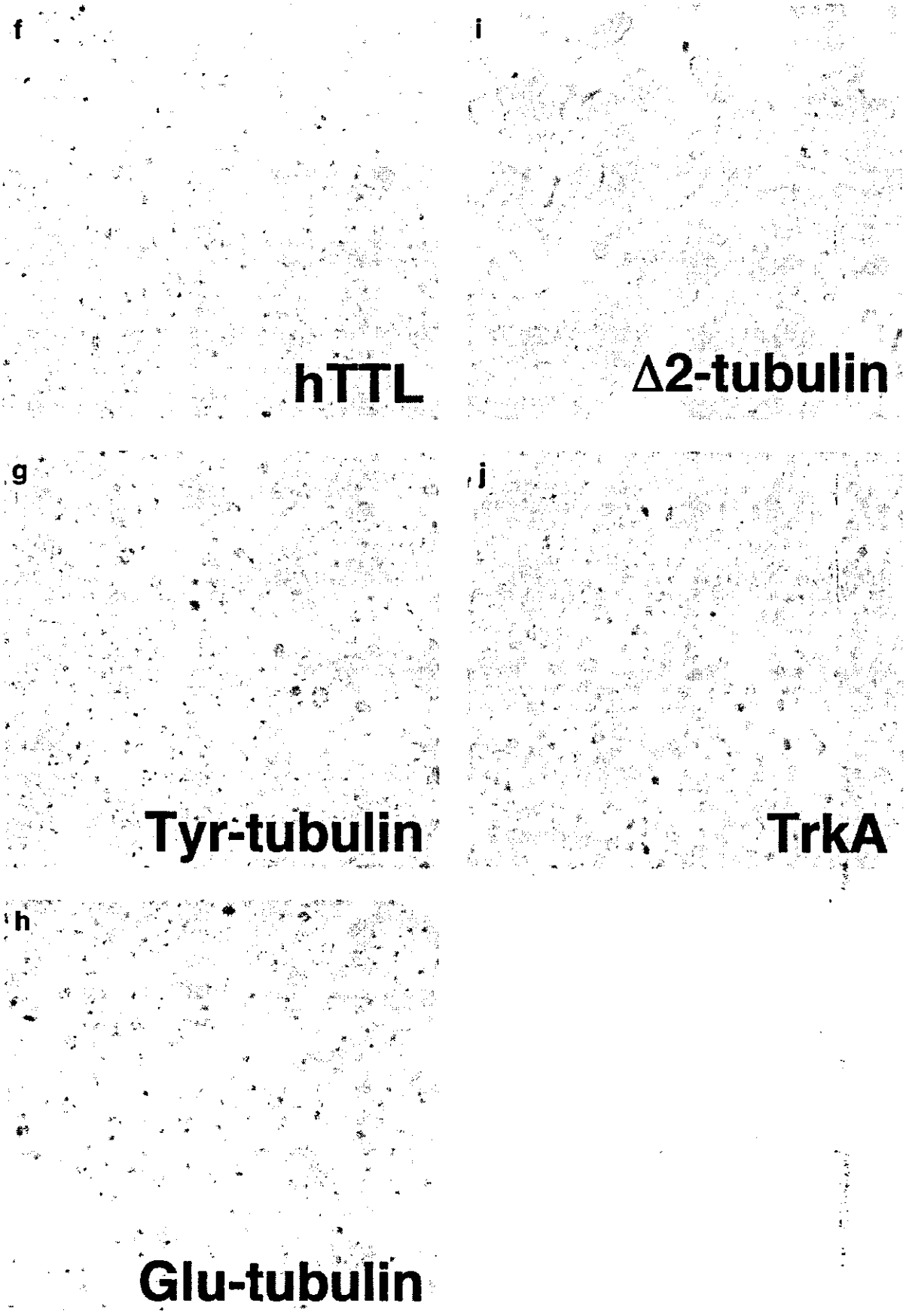

FIGURE 6 – (CONTINUED)

brain.[38] Therefore, many cellular stresses such as oxidative damage may trigger dysfunction of the tubulin/microtubule cytoskeletal system.

Our present study has shown that the decreases in Tyr-tubulin and Glu-tubulin are associated with relatively low levels of hTTL expression in unfavorable NBLs, which have lost a potency of neuronal differentiation and/or apoptosis. They are also correlated with decreased levels of TrkA, a high-affinity receptor for nerve growth factor, whose activation induces morphologic differentiation of NBL cells.[39] In addition, gradual upregulation of hTTL has been observed during induction of neuronal differentiation in RTBM1 cells treated with BMP2 or RA. These suggest that the induction of neuronal differentiation in NBL is accompanied with the activated tyrosination/detyrosination cycle regulated by increased level of hTTL enzyme, while the cycle is arrested by downregulation of hTTL in proliferating NBL cells, resulting in accumulation of Δ2-tubulin within the cells. Indeed, the expression levels of *hTTL* mRNA and Δ2-tubulin are significantly correlated with the prognosis of primary NBLs. This is consistent with the observation that TTL activity is lost, and conversely Δ2-tubulin is upregulated during the tumor cell growth.[19] Lafanechere *et al.*[19] have demonstrated by using mouse TTL null cells both *in vitro* and *in vivo* that mouse TTL activity is strongly decreased during tumor growth. Mas *et al.*[15] have also reported that, using rat *TTL* dominant negative mutant and an antisense cDNA of rat *TTL*, suppression of TTL activity induces 2- to 3-fold faster cell proliferation. Moreover, in human breast cancers, the accumulation of Glu-tubulin and Δ2-tubulin is correlated with poor prognosis by immunohistochemical approach.[28] It is noteworthy that our preliminary data using the microarray hybridized with total RNA obtained from 136 primary NBLs have shown that the gene with the highest score to predict prognosis of NBLs is α-tubulin (data not shown). Thus, the role of microtubule and its component, α-tubulin, is very important to define the biology as well as the aggressiveness of cancer cells.

In conclusion, we have identified a *human tubulin tyrosine ligase* gene and demonstrated its tissue distribution and correlation with neuronal differentiation. Since our data have suggested that the tyrosination cycle of α-tubulin is activated in differentiating NBLs but is inactivated in proliferating tumors, the cycle-related molecules including hTTL could be the targets for developing novel therapeutic strategies against advanced stages of NBL.

ACKNOWLEDGEMENTS

The authors thank Shigeru Sakiyama for critical reading of the manuscript, Naoko Sugimitsu for preparing RNA, Yuki Nakamura for DNA sequencing, Yoshiaki Okamoto for instructing quantitative real-time RT-PCR and Aiko Morohashi and Natsue Akao for technical assistance. The authors also thank the following institutions for providing surgical samples: First Department of Surgery, Hokkaido University School of Medicine; Department of Pediatrics, National Sapporo Hospital; Department of Pediatric Surgery, Tohoku University School of Medicine; Department of Surgery, Gunma Children's Medical Center; Department of Pediatrics, Pediatric Surgery and General Surgery, Jichi Medical University; Department of Hematology and Oncology, Saitama Children's Medical Center; Department of Pediatrics, Juntendo University School of Medicine; Department of Surgery, Kiyose Metropolitan Children's Hospital; Department of Surgery and Pathology, Chiba Children's Hospital; Department of Pediatric Surgery, Chiba University School of Medicine; Department of Pediatric Surgery, Kimitsu Central Hospital; Department of Pediatric Surgery, Niigata University School of Medicine; Department of Pediatrics and Pediatric Surgery, Aichi Medical University; Department of Pediatrics, Kyoto Prefectural Medical University; Tumor Board, Hyogo Children's Hospital; Department of Pediatrics and Pediatric Surgery, Kagoshima University School of Medicine; Department of Pediatric Surgery, Showa University School of Medicine; Department of Pediatrics, Oita University School of Medicine; Department of Pediatric Surgery, Ohta General Hospital; Department of Pediatrics, Ichinomiya City Hospital; Department of Pediatric Surgery, Osaka City General Hospital; Department of Pediatrics, Nihon University School of Medicine; Itabashi Hospital; Department of Pediatric Surgery, University of Tsukuba School of Medicine.

REFERENCES

1. MacRae TH. Tubulin post-translational modifications: enzymes and their mechanisms of action. Eur J Biochem 1997;244:265–78.
2. Zambito AM, Wolff J. Palmitoylation of tubulin. Biochem Biophys Res Commun 1997;239:650–4.
3. Barra HS, Arce CA, Argarana CE. Posttranslational tyrosination/detyrosination of tubulin. Mol Neurobiol 1988;2:133–53.
4. Luduena RF. Multiple forms of tubulin: different gene products and covalent modifications. Int Rev Cytol 1998;178:207–75.
5. Barra HS, Unates LE, Sayavedra MS, Caputto R. Capacities for binding amino acids by tRNAs from rat brain and their changes during development. J Neurochem 1972;19:2289–97.
6. Barra HS, Rodriguez JA, Arce CA, Caputto R. A soluble preparation from rat brain that incorporates into its own proteins (14 C)arginine by a ribonuclease-sensitive system and (14 C)tyrosine by a ribonuclease-insensitive system. J Neurochem 1973;20:97–108.
7. Barra HS, Arce CA, Rodriguez JA, Caputto R. Incorporation of phenylalanine as a single unit into rat brain protein: reciprocal inhibition by phenylalanine and tyrosine of their respective incorporations. J Neurochem 1973;21:1241–51.
8. Barra HS, Arce CA, Rodriguez JA, Caputto R. Some common properties of the protein that incorporates tyrosine as a single unit and the microtubule proteins. Biochem Biophys Res Commun 1974;60:1384–90.
9. Arce CA, Rodriguez JA, Barra HS, Caputo R. Incorporation of L-tyrosine, L-phenylalanine and L-3,4-dihydroxyphenylalanine as single units into rat brain tubulin. Eur J Biochem 1975;59:145–9.
10. Argarana CE, Arce CA, Barra HS, Caputto R. *In vivo* incorporation of [14C]tyrosine into the C-terminal position of the alpha subunit of tubulin. Arch Biochem Biophys 1977;180:264–8.
11. Preston SF, Deanin GG, Hanson RK, Gordon MW. The phylogenetic distribution of tubulin:tyrosine ligase. J Mol Evol 1979;13:233–44.
12. Gabius HJ, Graupner G, Cramer F. Activity patterns of aminoacyl-tRNA synthetases, tRNA methylases, arginyltransferase and tubulin: tyrosine ligase during development and ageing of *Caenorhabditis elegans*. Eur J Biochem 1983;131:231–4.
13. Stieger J, Wyler T, Seebeck T. Partial purification and characterization of microtubular protein from *Trypanosoma brucei*. J Biol Chem 1984;259:4596–602.
14. Ersfeld K, Wehland J, Plessmann U, Dodemont H, Gerke V, Weber K. Characterization of the tubulin-tyrosine ligase. J Cell Biol 1993;120:725–32.
15. Mas CR, Arregui CO, Filiberti A, Argarana CE, Barra HS. Cloning of rat olfactory bulb tubulin tyrosine ligase cDNA: a dominant negative mutant and an antisense cDNA increase the proliferation rate of cells in culture. Neurochem Res 2002;27:1453–8.
16. Paturle-Lafanechere L, Edde B, Denoulet P, Van Dorsselaer A, Mazarguil H, Le Caer JP, Wehland J, Job D. Characterization of a major brain tubulin variant which cannot be tyrosinated. Biochemistry 1991;30:10523–8.
17. Paturle-Lafanechere L, Manier M, Trigault N, Pirollet F, Mazarguil H, Job D. Accumulation of delta 2-tubulin, a major tubulin variant that cannot be tyrosinated, in neuronal tissues and in stable microtubule assemblies. J Cell Sci 1994;107:1529–43.
18. Lafanechere L, Job D. The third tubulin pool. Neurochem Res 2000;25:11–8.
19. Lafanechere L, Courtay-Cahen C, Kawakami T, Jacrot M, Rudiger M, Wehland J, Job D, Margolis RL. Suppression of tubulin tyrosine ligase during tumor growth. J Cell Sci 1998;111:171–81.
20. Ohira M, Morohashi A, Inuzuka H, Shishikura T, Kawamoto T, Kageyama H, Nakamura Y, Isogai E, Takayasu H, Sakiyama S, Suzuki Y, Sugano S, Goto T, Sato S, Nakagawara A. Expression profiling and characterization of 4200 genes cloned from primary neuroblastomas: identification of 305 genes differentially expressed between favorable and unfavorable subsets. Oncogene 2003;22:5525–36.
21. Ohira M, Morohashi A, Nakamura Y, Isogai E, Furuya K, Hamano S, Machida T, Aoyama M, Fukumura M, Miyazaki K, Suzuki Y, Sugano S, Hirato J, Nakagawara A. Neuroblastoma oligo-capping cDNA

project: toward the understanding of the genesis and biology of neuroblastoma. Cancer Lett 2003;197:63–8.
22. Brodeur GM, Pritchard J, Berthold F, Carlsen NL, Castel V, Castelberry RP, De Bernardi B, Evans AE, Favrot M, Hedborg F, kaneko M, Kemshead J, Lampert F, Lee RE, Look AT, Pearson AD, Philip T, Roald B, Sawada T, Seeger RC, Thuchida Y, Voute PA. Revisions of the international criteria for neuroblastoma diagnosis, staging, and response to treatment. J Clin Oncol 1993;11:1466–77.
23. Kaneko M, Nishihira H, Mugishima H, Ohnuma N, Nakada K, Kawa K, Fukuzawa M, Suita S, Sera Y, Tsuchida Y. Stratification of treatment of stage 4 neuroblastoma patients based on N-myc amplification status: Study Group of Japan for Treatment of Advanced Neuroblastoma, Tokyo, Japan. Med Pediatr Oncol 1998;31:1–7.
24. Hishiki T, Nimura Y, Isogai E, Kondo K, Ichimiya S, Nakamura Y, Ozaki T, Sakiyama S, Hirose M, Seki N, Takahashi H, Ohnuma N, Tanabe M, Nakagawara A. Glial cell line-derived neurotrophic factor/neurturin-induced differentiation and its enhancement by retinoic acid in primary human neuroblastomas expressing c-Ret, GFR alpha-1, and GFR alpha-2. Cancer Res 1998;58:2158–65.
25. Chomczynski P, Sacchi N. Single-step method of RNA isolation by acid guanidinium thiocyanate-phenol-chloroform extraction. Anal Biochem 1987;162:156–9.
26. Shimada H, Ambros IM, Dehner LP, Hata J, Joshi VV, Roald B, Stram DO, Gerbing RB, Lukens JN, Matthay KK, Castleberry RP. The International Neuroblastoma Pathology Classification (the Shimada system). Cancer 1999;86:364–72.
27. Goto S, Umehara S, Gerbing RB, Stram DO, Brodeur GM, Seeger RC, Lukens JN, Matthay KK, Shimada H. Histopathology (International Neuroblastoma Pathology Classification) and MYCN status in patients with peripheral neuroblastic tumors: a report from the Children's Cancer Group. Cancer 2001;92:2699–708.
28. Mialhe A, Lafanechere L, Treilleux I, Peloux N, Dumontet C, Bremond A, Panh MH, Payan R, Wehland J, Margolis RL, Job D. Tubulin detyrosination is a frequent occurrence in breast cancers of poor prognosis. Cancer Res 2001;61:5024–7.
29. Iwasaki S, Hattori A, Sato M, Tsujimoto M, Kohno M. Characterization of the bone morphogenetic protein-2 as a neurotrophic factor: induction of neuronal differentiation of PC12 cells in the absence of mitogen-activated protein kinase activation. J Biol Chem 1996;271:17360–5.
30. Nakamura Y, Ozaki T, Koseki H, Nakagawara A, Sakiyama S. Accumulation of p27 KIP1 is associated with BMP2-induced growth arrest and neuronal differentiation of human neuroblastoma-derived cell lines. Biochem Biophys Res Commun 2003;307:206–13.
31. Arregui CO, Mas CR, Argarana CE, Barra HS. Tubulin tyrosine ligase: protein and mRNA expression in developing rat skeletal muscle. Dev Growth Differ 1997;39:167–78.
32. Eiserich JP, Estevez AG, Bamberg TV, Ye YZ, Chumley PH, Beckman JS, Freeman BA. Microtubule dysfunction by posttranslational nitrotyrosination of alpha-tubulin: a nitric oxide-dependent mechanism of cellular injury. Proc Natl Acad Sci USA 1999;96:6365–70.
33. Kalisz HM, Erck C, Plessmann U, Wehland J. Incorporation of nitrotyrosine into alpha-tubulin by recombinant mammalian tubulin-tyrosine ligase. Biochim Biophys Acta 2000;1481:131–8.
34. Bisig CG, Purro SA, Contin MA, Barra HS, Arce CA. Incorporation of 3-nitrotyrosine into the C-terminus of alpha-tubulin is reversible and not detrimental to dividing cells. Eur J Biochem 2002;269:5037–45.
35. Ischiropoulos H. Biological tyrosine nitration: a pathophysiological function of nitric oxide and reactive oxygen species. Arch Biochem Biophys 1998;3561–611.
36. Hensley K, Maidt ML, Yu Z, Sang H, Markesbery WR, Floyd RA. Electrochemical analysis of protein nitrotyrosine and dityrosine in the Alzheimer brain indicates region-specific accumulation. J Neurosci 1998;18:8126–32.
37. Beal MF, Ferrante RJ, Browne SE, Matthews RT, Kowall NW, Brown RH Jr. Increased 3-nitrotyrosine in both sporadic and familial amyotrophic lateral sclerosis. Ann Neurol 1997;42:644–54.
38. Ishida Y, Ichimura T, Sumi H, Horigome T, Omata S. Methylmercury alters the tyrosination status of tubulin in the brains of acutely intoxicated rats. Toxicology 1997;122:171–81.
39. Nakagawara A, Arima-Nakagawara M, Scavarda NJ, Azar CG, Cantor AB, Brodeur GM. Association between high levels of expression of the TRK gene and favorable outcome in human neuroblastoma. N Engl J Med 1993;328:847–54.

Decreased expression of the candidate tumor suppressor gene *ING1* is associated with poor prognosis in advanced neuroblastomas

MASATO TAKAHASHI[1,2], TOSHINORI OZAKI[1], SATORU TODO[2] and AKIRA NAKAGAWARA[1]

[1]Division of Biochemistry, Chiba Cancer Center Research Institute, 666-2 Nitona, Chuoh-ku, Chiba 260-8717;
[2]First Department of Surgery, Hokkaido University School of Medicine, N15 W7, Kita-ku, Sapporo 060-8638, Japan

Received January 27, 2004; Accepted March 30, 2004

Abstract. *ING1* has been identified as a novel candidate tumor suppressor gene using a genetic suppressor element (GSE) strategy. Ectopic expression of *ING1* in mammalian cultured cells causes cell cycle arrest and apoptosis through a p53-dependent and/or p53-independent pathway. However, there has been no report on the prognostic significance of the *ING1* expression level in human cancers, though the expression of the wild-type *ING1* gene is significantly decreased in breast, lymphoid and gastric cancers as compared with their corresponding normal tissues. In order to explore the possible involvement of *ING1* in tumorigenesis of neuroblastoma, we examined the expression levels of *ING1* mRNA in 32 primary neuroblastomas by using a quantitative real-time PCR. *ING1* mRNA was expressed independently of the disease stages. However, low levels of *ING1* mRNA were significantly associated with a poor prognosis (log-rank test, p=0.017). Multivariate analysis showed that the expression level of *ING1* was closely related to survival (p=0.020), even after controlling with age (p=0.008) or stage (p=0.025), while it was only marginally significant after controlling with *TrkA* expression (p=0.063). Mutation analysis revealed that there was no mutation or deletion of the *ING1* gene except 1 silent mutation at codon 188 in primary neuroblastomas examined. Taken together, our results suggest for the first time that a decreased level of *ING1* expression is a novel indicator of poor prognosis in advanced stages of neuroblastoma, and that ING1 may play a crucial role in genesis and progression of neuroblastoma.

Introduction

Neuroblastoma, which is derived from the sympathoadrenal lineage of the neural crest, is one of the most common pediatric solid tumors (1). Neuroblastoma is an enigmatic tumor and shows distinct biology in 2 subsets. A subset of tumors in early stages has favorable prognosis and usually occurs in patients <1 year of age. They have no amplification of the *MYCN* oncogene and often differentiate and/or regress spontaneously. In contrast, the other is a subset of tumors in the advanced stages with poor prognosis, which usually possesses *MYCN* amplification and allelic loss in the distal region of the short arm of chromosome 1. However, there is an intermediate type of neuroblastoma which displays advanced phenotypes but has no *MYCN* amplification (2). From the clinical point of view, the latter type of neuroblastoma is the most problematic, and it is quite difficult to decide which therapeutic strategy should be chosen.

ING1 has been identified as a novel candidate tumor suppressor gene by using a novel strategy, which combines a subtractive hybridization and *in vivo* selection system (genetic suppressor elements method, GSE) (3,4). The *ING1* gene encodes a nuclear protein with a molecular mass of 33 kDa, which exhibits no significant homology with known proteins filed in the public databases. According to the recent reports, there exist at least 3 *ING1* variants arising from alternative splicing of mRNA (5,6). It has been mapped to human chromosome 13q33-q34, the region of which is known to be involved in the progression of various cancers (7-10). Expression of *ING1* is regulated in a cell cycle-dependent manner, reaching a maximal level during the S-phase (11-13). Ectopic expression of *ING1* in certain mammalian cultured cells results in a cell cycle arrest at the G0/G1 phase, suggesting that ING1 acts as a potent growth regulator (4). Furthermore, the physical and functional interaction of ING1 with tumor suppressor p53 has been reported and this could be one of the key mechanisms of the p53-mediated growth regulation (14). In addition, mutation of *ING1* which generates a truncated protein has been found in one of the neuroblastoma cell lines (4), suggesting that ING1 might be involved in genesis and/or progression of neuroblastoma.

To confirm this possibility, we performed mutation analysis of the *ING1* gene and also examined the expression levels of *ING1* mRNA in 32 primary neuroblastoma tissues. Although we did not detect any mutations or deletions, we found a significant decrease in the expression levels of *ING1* mRNA

Correspondence to: Dr Akira Nakagawara, Division of Biochemistry, Chiba Cancer Center Research Institute, 666-2 Nitona, Chuoh-ku, Chiba 260-8717, Japan
E-mail: akiranak@chiba-cc ri.chuo.chiba.jp

Key words: ING1, neuroblastoma, p53, prognostic factor

in neuroblastoma tissues derived from patients who died of the disease. Thus, our present study suggests that the decreased level of *ING1* expression is a novel indicator of poor prognosis in advanced neuroblastoma.

Materials and methods

Patients and tumor tissues. Among 32 samples, 11 cases were identified by a mass screening program for neuroblastoma that began in 1985 in Japan. Eight tumors were obtained from patients treated at the Pediatric Oncology Group Institutions or other institutions in the United States. All tumors were diagnosed by histologic assessment. These consisted of 4 ganglioneuroblastomas and 28 neuroblastomas, all of which were considered neuroblastomas in these analyses. Staging was performed according to the staging system described by Evans *et al* (15), and identified 9 stage I, 4 stage II, 7 stage III, 5 stage IV and 7 stage IVs. All of the patients were treated according to previously described protocols (16-20). Despite differences between the protocols for the Japanese patients and those for the patients treated by the Pediatric Oncology Group, drugs and their doses were similar and the stage-specific survival rates obtained by these 2 groups did not differ significantly (data not shown). The median follow-up period after diagnosis was 26 months (range, 7-63). None of the patients underwent bone marrow transplantation.

Southern hybridization. The *MYCN* gene amplification was examined by Southern analysis. High molecular weight genomic DNA prepared from frozen neuroblastoma tissues was digested completely with *Eco*RI, separated by 1% agarose gel electrophoresis and transferred onto a nylon membrane filter. The filter was fixed by UV irradiation and hybridized at 42°C in a solution containing 6X SSC, 5x Denhardt's solution, 0.5% SDS and ^{32}P-labeled *MYCN* DNA. After hybridization, the filter was washed extensively at 50°C in 0.1X SSC containing 0.1% sarcosine and exposed to X-ray film with an intensifying screen at -70°C. The *MYCN* copy number was determined as described previously (21).

Northern blot analysis. Total RNA was extracted from 0.5-1.0 g of frozen neuroblastoma tissues using a standard guanidine thiocyanate extraction procedure (22). Total RNA (20 μg) was electrophoresed in 1% agarose gel under denaturing conditions and transferred by capillary onto nylon membrane filters. Hybridization was conducted at 42°C under the standard conditions in 6X SSC, 5X Denhardt's solution, 0.5% SDS and a radio-labeled cDNA probe for *TrkA* and *p53*. After hybridization, filters were washed at room temperature in 2X SSC/0.1% sarcosine followed by 2 washes at 50°C in 0.1X SSC containing 0.1% sarcosine and then exposed to X-ray film with an intensifying screen at -70°C. To normalize the expression level of genes of interest, filters were stripped of probes and rehybridized with a radio-labeled cDNA encoding *β-actin*. The intensity of each specific band was measured by a densitometric scanning, and the expression level of each gene was expressed as arbitrary density units. The distinction between high and low level of *TRK-A* expression was based on the value of the histogram that gave the best natural separation (23).

Quantitative RT-PCR analysis. The expression level of *ING1* was measured by a real-time RT-PCR method (24). Total RNA (2 μg) was converted to first-strand cDNA using Superscript II reverse transcriptase (Life Technologies, Rockville, MD, USA). The PCR amplification was performed with the following primers: *ING1* sense (725F) (5'-AGATGATCGGCTGCGAC AA-3') and antisense (1038R) (5'-TCCCTATGAAAGGA ATGGTTCC-3'). The probe oligonucleotide (952T) (5'-TACATTGCCTTTGTTGAGGTGCAT-3') which hybridizes with the target sequences of the PCR products, was labeled with a reporter fluorescent dye (FAM, 6-carboxy-fluorescein) and a quencher fluorescent dye (TAMRA, 6-carboxytetramethyl-rhodamine) at its 5'- and 3'-end, respectively. PCR was carried out in a 25 μl reaction mixture containing 0.2 μM of each primer, 0.3 mM dATP, 0.3 mM dGTP, 0.3 mM dCTP, 0.6 mM dUTP instead of dTTP, 4 mM $Mn(OAc)_2$, 1X TaqMan EZ Buffer A, 0.25 units of AmpErase uracil N-glycosylase, 0.625 units of AmpliTaq Gold and 0.1 μM probe oligonucleotide. Reaction mixtures were pre-incubated at 50°C for 2 min, 95°C for 5 min and then subjected to 40 cycles of 95°C for 20 sec and 62°C for 1 min using ABI Prism 7700 Sequence Detector (PE Applied Biosystems). During the PCR amplification, the fluorescent-labeled probe was hydrolyzed by the activity of AmpliTaq Gold and the reporter dye was released from the probe oligonucleotide. The resulting increase in the reporter fluorescent emission was monitored in real-time. The expression level of *ING1* was normalized to that of *β-actin* which was detected by the same real-time RT-PCR method.

RT-PCR SSCP analysis and DNA sequencing. For the detection of *ING1* mutation, we designed 4 primer sets which cover the entire coding region of human *ING1*. the reaction mixture contained 1 μl of the cDNA synthesized, 1 μM of each primer, 200 nM dNTPs, 1X reaction buffer, 0.15 units DNA polymerase (Expand High Fidelity PCR system) and [α-^{32}P]dCTP. PCR was performed as follows: pre-heating at 96°C for 3 min followed by 35 cycles of 96°C for 30 sec, 56°C for 30 sec and 72°C for 30 sec with final extension at 72°C for 5 min. PCR products were mixed with 1/10 volume of a loading buffer containing 95% formamide, 20 mM EDTA, 0.05% bromophenol blue and 0.05% xylene cyanol, denatured at 98°C for 5 min, and quenched on ice. Electrophoresis was carried out on 5% polyacrylamide gel with 5% glycerol at room temperature at 200 V for 15 h. After electrophoresis, the gel was dried and exposed to X-ray film with an intensifying screen at -70°C.

To determine nucleotide sequences of PCR products, they were purified by the GenElute Agarose Spin Column (Supelco, Bellefonte, PA, USA), subcloned into pGEM-T Easy Vector (Promega, Madison, WI, USA), and sequenced by the dideoxy chain termination method using the ABI Prism 377 DNA sequencer (Perkin-Elmer, Foster City, CA, USA).

Statistical analysis. A possible association between the *ING1* expression level and all prognostic factors was investigated using the Mann-Whitney U test. Pearson correlation with Bonferroni-adjusted significance levels were calculated between expression levels of all genes examined. Since the values of mRNA expression were skewed, a log or Box-cox

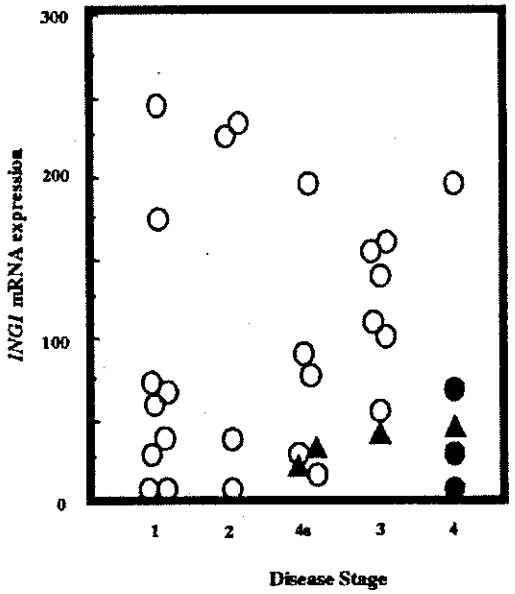

Figure 1. Expression of *ING1* mRNA in primary neuroblastomas. Total RNA was prepared from the indicated primary neuroblastoma tissues, and subjected to a quntitative real-time RT-PCR analysis as described under Materials and methods. The ratios of *ING1* mRNA levels to *β-actin* mRNA levels were quantified and are indicated as a fold change on the y axis. Nine in stage I, 4 in stage II, 7 in stage III, 5 in stage IV and 7 in stage IVs. (○), alive; (●), dead with single copy of *MYCN*; (▲), dead with *MYCN* amplification.

transformation was used to achieve the normality when calculating correlation coefficients. Comparisons between 2 clinical or biological variables were carried out using the χ^2 analysis. The Kaplan-Meier life table analysis was applied to compare individual variables and survival, and different survival curves were compared using the log-rank test. Cox regression models were used to explore the association between the expression of *ING1* and age, tumor stage, *MYCN*, *TRK-A* or survival. We considered $p>0.05$ to be significant. Statistical analyses were performed using the StatView version 4.5 (Abacus Concept Inc. Berkeley, CA, USA) and Stata version 6.0. (Stata Corporation, TX, USA).

Results

Mutation analysis of ING1 gene in human neuroblastoma. Recently, it has been reported that one of the human neuroblastoma cells, SK-N-SH, carries a mutation of the *ING1* gene, which generates a truncated form of *ING1* (4). To search for mutation of the *ING1* gene in 32 primary neuroblastoma tissues, we performed RT-PCR-single strand conformation polymorphism (SSCP) analysis, followed by subsequent DNA sequencing according to the procedure as described previously (25,26). Among 32 samples examined, the PCR product amplified from 1 case of neuroblastoma in stage I displayed an aberrantly migrating band, however, DNA sequencing analysis revealed that this aberrant band reflected a silent mutation at codon 188 [Ser188Ser (TCG-TCA)] (data not shown).

Down-regulation of ING1 mRNA is associated with unfavorable prognosis of neuroblastoma. We then examined

Table I. The results of log-rank tests for conventional prognostic factors and expression of *ING1* and *p53* in 32 primary neuroblastomas.

Variable	Number of subjects	Number of deaths (%)	Number of expected deaths	p-value
ING1 expression				.017
Low	16	6 (37.5)	2.96	
High	16	1 (6.3)	4.04	
p53 expression				.250
Not expressed	7	2 (28.6)	0.98	
Expressed	22	3 (13.6)	4.02	
Age				.001
<1 year	19	1 (5.3)	4.93	
>1 year	12	6 (50.0)	2.07	
Origin				.077
Adrenal gland	24	7 (100)	4.89	
Others	8	0 (0)	2.11	
Disease stage				.044
I+II+IVs	20	2 (10.0)	4.53	
III+IV	12	5 (41.7)	2.47	
MYCN copy number				<.0001
Amplified	4	4 (100)	0.39	
Single copy	28	3 (10.7)	6.61	
Trk-A expression				.0032
Low	6	3 (50.0)	0.78	
High	24	2 (8.3)	4.28	

ING1 expression levels in primary neuroblastomas because epigenetic regulation of the tumor suppressor genes are involved in the genesis and/or progression of many human cancers (27). Since the expression levels of *ING1* mRNA were below the detectable levels by Northern blot hybridization, we performed a quantitative real-time RT-PCR (24) to measure its expression levels in 32 neuroblastoma tissues. The threshold cycle number value (C_T), indicating the relative levels of *ING1* mRNA (after normalization to that of *β-actin* mRNA) was in the range of 0-250 (median value, 64). As shown in Fig. 1, there were no statistically significant differences in expression levels of *ING1* mRNA among the disease stages (mean ± SEM; stage I, 79±27, n=9; stage II, 126±59, n=4; stage IVs, 67±24, n=7; stage III, 110±17, n=7; stage IV, 70±33, n=5; $p>0.05$). Note that *ING1* expression levels were significantly decreased in the tumors obtained from the patients who died of the disease (mean ± SEM; 36±8, n=7) as compared with those patients who were alive (101±15, n=25) (Mann-Whitney U test, $p=0.043$). Then, the patients were divided into 2 groups according to the median value of *ING1* mRNA expression in the tumor. The log-rank test showed that the prognosis of the patients with decreased expression of *ING1* was significantly poor ($p=0.017$) (Table I and Fig. 2).

The expression of p53 was not correlated with the prognosis of neuroblastoma. Since ING1 has been shown to modulate the function of p53 through the physical interaction with p53

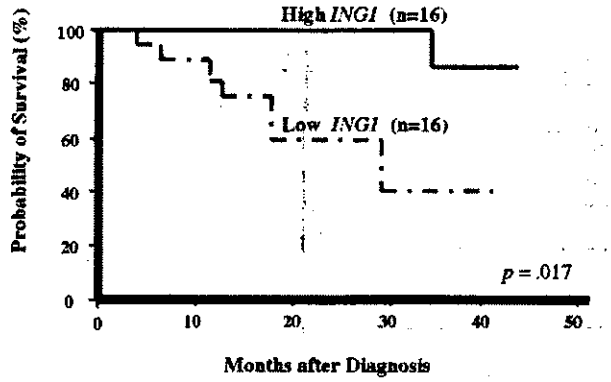

Figure 2. *ING1* mRNA expression and survival curves calculated by the Kaplan-Meier method. Kaplan-Meier life table analysis was used to compare the individual variables and survival, and different survival curves were compared using the log-rank test. Statistical analyses were performed using the StatView viersion 4.5 and Stata version 6.0. (—), A group of patients with high levels of *ING1* expression; (- • - • -), a group of patients with low levels of *ING1* expression.

Table II. Cox regression models using dichotomous factors of age, disease stage, *MYCN* amplification and expression of *Trk-A* and *ING1*.

Factor	n	p-value	HR (95% CI)
Age (≥1 vs. <1 year)	31	.013	14.6 (1.75-121)
Stage (III+IV vs. I+II+IVs)	32	.069	4.6 (0.89-23.6)
MYCN ampl. (>1 vs. 1 copy)	32	<.0005	55.8 (6.01-518)
Trk-A exp. (low vs. high)	30	.016	9.4 (1.53-57.8)
ING1 exp. (low vs. high)	32	.046	9.0 (1.04-77.2)
ING1 exp. (low vs. high)	31	.022	27.1 (1.61-455)
Age (≥1 vs. <1 year)		.008	24.3 (2.32-255)
ING1 exp. (low vs. high)	32	.023	15.7 (1.47-167)
Stage (III+IV vs. I+II+IVs)		.025	7.7 (1.30-45.2)
ING1 exp. (low vs. high)	30	.063	12.9 (0.87-190)
Trk-A exp. (low vs. high)		.017	17.3 (1.68-179)

All variables with 2 categories; HR, hazard ratio shows the relative risk of death of first category relative to the second; CI, confidence interval.

(14), we also examined the expression levels of *p53* in the same neuroblastoma tissues by Northern blot hybridization. The expression of *β-actin* mRNA served as an internal control, and the patients were divided into 2 groups with detectable (high) and undetectable (low) expression of *p53*. As shown in Table I, *p53* expression was not significantly associated with the prognosis of neuroblastoma (p=0.25). These results suggest that the decreased expression of *ING1* but not of *p53* is correlated with the unfavorable prognosis of neuroblastoma.

ING1 expression is an independent prognostic indicator for neuroblastoma. We then performed a multivariate analysis of the prognostic factors for neuroblastoma including *ING1* expression. As shown in Table II, the predictive importance of *ING1* expression for survival was demonstrated after controlling patient's age (p=0.022) and disease stage (p=0.023), whereas *ING1* expression was marginally significant (p=0.063) after controlling *TrkA* expression. This implied that *ING1* expression may be a prognostic indicator which is independent on age and stage, but that it may be weakly associated with *TrkA* expression in predicting the prognosis of neuroblastoma.

Discussion

In the present study, we have searched for mutations of the *ING1* gene, and examined the expression levels of *ING1* mRNA in 32 primary neuroblastoma tissues. Although we did not detect any mutations with amino acid substitutions, we found that the expression levels of *ING1* mRNA were significantly reduced in unfavorable neuroblastoma, and this marked down-regulation was associated with the poor prognosis of neuroblastoma. Our present results represent an initial step toward understanding the biological significance of *ING1* in neuroblastoma.

Recently, it has been shown that ING1 has an ability to promote cell cycle arrest and apoptosis in certain mammalian cultured cells (14,28). Garkavtsev *et al* found a truncated form of *ING1* protein in neuroblastoma cell lines, which might be generated by a structural rearrangement or a deletion that occurred within the *ING1* gene (4). It remains unknown whether the truncated ING1 protein retains the ability to inhibit cell cycle progression, and whether there exists a loss of function mutations of *ING1* in primary neuroblastoma, it is likely that ING1 might act as a candidate tumor suppressor for neuroblastoma. Consistent with the recent reports showing that *ING1* is rarely mutated in human malignancies (5,29-31), our mutation analysis indicated that *ING1* is infrequently mutated in primary neuroblastomas and thus it might not function as a tumor suppressor in the classic manner (32). Note that our quantitative real-time RT-PCR analysis revealed that the expression levels of *ING1* mRNA were reduced in unfavorable neuroblastomas, and that this down-regulation was significantly correlated with the poor prognosis of neuroblastoma. Although the number of tumor samples used in this study was relatively small, the statistical significance of the traditional prognostic factors including patient's age (p=0.001), disease stage (p= 0.044), *MYCN* amplification (p<0.0001) and *TrkA* expression (p=0.0032) were in good agreement with those reproducibly documented (15,33,34). Thus, our present results suggest that *ING1* expression is a novel prognostic indicator for neuroblastomas especially in advanced stages. In order to design a new therapeutic strategy against aggressive neuroblastoma, it will be necessary to clarify the molecular mechanisms of this transcriptional down-regulation of the *ING1* gene in unfavorable neuroblastoma.

There is considerable evidence that the p53 pathway is not exclusively responsible for the genesis and/or progression of neuroblastoma. For example, *p53* is infrequently mutated in primary neuroblastomas, and wild-type p53 is localized largely in cytoplasm of primary tumors as well as neuroblastoma-derived cell lines (35-39). In addition, our present study indicated that the expression levels of *p53* mRNA is not associated with the prognosis of neuroblastoma. On the other hand, it has been shown that p53 plays an important

role in inducing neuronal cell death of sympathetic neurons, from which neuroblastoma originates (40). Recently, Nakagawa *et al* reported that during cisplatin-mediated cell death in neuroblastoma-derived SH-SY5Y cells, endogenous p53 accumulated at a protein level, suggesting that the p53 pathway is closely involved in DNA damage-induced neuroblastoma cell death (41). Previous studies have demonstrated that ING1 physically interacts with p53, and thereby acts as a cofactor of p53 to enhance its ability to transactivate downstream target genes as well as to inhibit cell cycle progression (14,42). It is likely that the reduced expression of *ING1* could down-regulate the pro-apoptotic function of p53 and thereby promote neuroblastoma cell growth. To confirm this possibility, further studies are necessary.

Acknowledgements

We are grateful to S. Sakiyama and S. Ichimiya for valuable discussions, and A. Morohashi for preparing RNA. We thank Y. Nakamura and M. Nagano for assistance in quantitative RT-PCR analysis. This work was supported in part by a Grant-in-Aid from the Ministry of Health and Welfare for a New 10-Year Strategy for Cancer Control, a Grant-in-Aid from the Ministry of Health and Welfare for the Study Group for Treatment of Advanced Neuroblastoma, Uehara Foundation, and a Grant-in-Aid for Scientific Research from the Ministry of Education, Science, Sports and Culture, Japan. Masato Takahashi is an awardee of the Research Resident Fellowship from the Foundation for Promotion of Cancer Research in Japan.

References

1. Bolande R: The neurocristopathies: a unifying concept of disease arising in neural crest maldevelopment. Human Pathol 5: 409-424, 1974.
2. Brodeur GM and Nakagawara A: Molecular basis of clinical heterogeneity in neuroblastoma. Am J Pediatr Hematol Oncol 14: 111-116, 1992.
3. Roninson IB, Gudkov AV, Holzmayer TA, Kirschling DJ, Kazarov AR, Zelnick CR, Mazo IA, Axenovich S and Thimmapaya R: Genetic suppressor elements: new tools for molecular oncology - Thirteenth Cornelius P. Rhoads Memorial Award Lecture. Cancer Res 55: 4023-4028, 1995.
4. Garkavtsev I, Kazarov A, Gudkov A and Riabowol K: Suppression of the novel growth inhibitor p33*ING1* promotes neoplastic transformation. Nat Genet 14: 415-420, 1996.
5. Gunduz M, Ouchida M, Fukushima K, Hanafusa H, Etani T, Nishioka S, Nishizaki K and Shimizu K: Genomic structure of the human *ING1* gene and tumor-specific mutations detected in head and neck squamous cell carcinomas. Cancer Res 60: 3143-3146, 2000.
6. Saito A, Furukawa T, Fukushige S, Koyama S, Hoshi M, Hayashi Y and Horii A: p24/*ING1*-ALT1 and p47/*ING1*-ALT2, distinct alternative transcripts of p33/*ING1*. J Hum Genet 45: 177-181, 2000.
7. Motomura K, Nishisho I, Takai S, Tateishi H, Okazaki M, Yamamoto M, Miki T, Honjo T and Mori T: Loss of alleles at loci on chromosome 13 in human primary gastric cancers. Genomics 2: 180-184, 1988.
8. Ried T, Petersen I, Holtgreve-Grez H, Speicher MR, Schrock E, du Manoir S and Cremer T: Mapping of multiple DNA gains and losses in primary small cell lung carcinomas by comparative genomic hybridization. Cancer Res 54: 1801-1806, 1994.
9. Maestro R, Piccinin S, Doglioni C, Gasparotto D, Vukosavljevic T, Sulfaro S, Barzan L and Boiocchi M: Chromosome 13q deletion mapping in head and neck squamous cell carcinomas: identification of two distinct regions of preferential loss. Cancer Res 56: 1146-1150, 1996.
10. Hyytinen ER, Frierson HF Jr, Boyd JC, Chung LW and Dong JT: Three distinct regions of allelic loss at 13q14, 13q21-22, and 13q33 in prostate cancer. Genes Chromosomes Cancer 25: 108-114, 1999.
11. Garkavtsev I, Demetrick D and Riabowol K: Cellular localization and chromosome mapping of a novel candidate tumor suppressor gene (*ING1*). Cytogenet Cell Genet 76: 176-178, 1997.
12. Zeremski M, Horrigan SK, Grigorian IA, Westbrook CA and Gudkov AV: Localization of the candidate tumor suppressor gene *ING1* to human chromosome 13q34. Somat Cell Mol Genet 23: 233-236, 1997.
13. Garkavtsev I and Riabowol K: Extension of the replicative life span of human diploid fibroblasts by inhibition of the p33*ING1* candidate tumor suppressor. Mol Cell Biol 17: 2014-2019, 1997.
14. Garkavtsev I, Grigorian IA, Ossovskaya VS, Chernov MV, Chumakov PM and Gudkov AV: The candidate tumour suppressor p33*ING1* cooperates with p53 in cell growth control. Nature 391: 295-298, 1998.
15. Evans AE, D'Angio GJ and Randolph J: A proposed staging for children with neuroblastoma. Children's cancer study group A. Cancer 27: 374-378, 1971.
16. Ikeda K, Nakagawara A, Yano H, Akiyama H, Tasaka H, Ueda K, Hara T, Ishii E, Ohgami H, Sera Y, *et al*: Improved survival rates in children over 1 year of age with stage III or IV neuroblastoma following an intensive chemotherapeutic regimen. J Pediatr Surg 24: 189-193, 1989.
17. Nitschke R, Smith EI, Altshuler G, Altmiller D, Shuster J, Green A, Castleberry R, Hayes FA, Golembe B and Ducos R: Postoperative treatment of nonmetastatic visible residual neuroblastoma: a Pediatric Oncology Group study. J Clin Oncol 9: 1181-1188, 1991.
18. Castleberry RP, Kun LE, Shuster JJ, Altshuler G, Smith IE, Nitschke R, Wharam M, McWilliams N, Joshi V and Hayes FA: Radiotherapy improves the outlook for patients older than 1 year with Pediatric Oncology Group stage C neuroblastoma. J Clin Oncol 9: 789-795, 1991.
19. Look AT, Hayes FA, Shuster JJ, Douglass EC, Castleberry RP, Bowman LC, Smith EI and Brodeur GM: Clinical relevance of tumor cell ploidy and N-myc gene amplification in childhood neuroblastoma: a Pediatric Oncology Group study. J Clin Oncol 9: 581-591, 1991.
20. Hirai M, Yoshida S, Kashiwagi H, Kawamura T, Ishikawa T, Kaneko M, Ohkawa H, Nakagawara A, Miwa M and Uchida K: 1q23 gain is associated with progressive neuroblastoma resistant to aggressive treatment. Genes Chromosomes Cancer 25: 261-269, 1999.
21. Brodeur GM, Seeger RC, Schwab M, Varmus HE and Bishop JM: Amplification of N-myc in untreated human neuroblastomas correlates with advanced disease stage. Science 224: 1121-1124, 1984.
22. Chomczynski P and Sacchi N: Single-step method of RNA isolation by acid guanidinium thiocyanate-phenol-chloroform extraction. Anal Biochem 162: 156-159, 1987.
23. Nakagawara A, Arima M, Azar CG, Scavarda NJ and Brodeur GM: Inverse relationship between trk expression and N-myc amplification in human neuroblastomas. Cancer Res 52: 1364-1368, 1992.
24. Heid CA, Stevens J, Livak KJ and Williams PM: Real-time quantitative PCR. Genome Res 6: 986-994, 1996.
25. Ichimiya S, Nimura Y, Kageyama H, Takada N, Sunahara M, Shishikura T, Nakamura Y, Sakiyama S, Seki N, Ohira M, Kaneko Y, McKeon F, Caput D and Nakagawara A: p73 at chromosome 1p36.3 is lost in advanced stage neuroblastoma but its mutation is infrequent. Oncogene 18: 1061-1066, 1999.
26. Sunahara M, Shishikura T, Takahashi M, Todo S, Yamamoto N, Kimura H, Kato S, Ishioka C, Ikawa S, Ikawa Y and Nakagawara A: Mutational analysis of p51A/TAp63gamma, a p53 homolog, in non-small cell lung cancer and breast cancer. Oncogene 18: 3761-3765, 1999.
27. Jirtle RL: Genomic imprinting and cancer. Exp Cell Res 248: 18-24, 1999.
28. Helbing CC, Veillette C, Riabowol K, Johnston RN and Garkavtsev I: A novel candidate tumor suppressor, *ING1*, is involved in the regulation of apoptosis. Cancer Res 57: 1255-1258, 1997.
29. Toyama T, Iwase H, Watson P, Muzik H, Saettler E, Magliocco A, DiFrancesco L, Forsyth P, Garkavtsev I, Kobayashi S and Riabowol K: Suppression of *ING1* expression in sporadic breast cancer. Oncogene 18: 5187-5193, 1999.

30. Campos EI, Cheung KJ Jr, Murray A, Li S and Li G: The novel tumour suppressor gene *ING1* is overexpressed in human melanoma cell lines. Br J Dermatol 146: 574-580, 2002.
31. Chen B, Campos EI, Crawford R, Martinka M and Li G: Analyses of the tumour suppressor *ING1* expression and gene mutation in human basal cell carcinoma. Int J Oncol 22: 927-931, 2003.
32. Knudson AG Jr: Mutation and cancer: statistical study of retinoblastoma. Proc Natl Acad Sci USA 68: 820-823, 1971.
33. Coldman AJ, Fryer CJ, Elwood JM and Sonley MJ: Neuroblastoma: influence of age at diagnosis, stage, tumor site, and sex on prognosis. Cancer 46: 1896-1901, 1980.
34. Nakagawara A, Arima-Nakagawara M, Scavarda NJ, Azar CG, Cantor AB and Brodeur GM: Association between high levels of expression of the TRK gene and favorable outcome in human neuroblastoma. N Engl J Med 328: 847-854, 1993.
35. Vogan K, Bernstein M, Leclerc JM, Brisson L, Brossard J, Brodeur GM, Pelletier J and Gros P: Absence of p53 gene mutations in primary neuroblastomas. Cancer Res 53: 5269-5273, 1993.
36. Castresana JS, Bello MJ, Rey JA, Nebreda P, Queizan A, Garcia-Miguel P and Pestana A: No TP53 mutations in neuroblastomas detected by PCR-SSCP analysis. Genes Chromosomes Cancer 10: 136-138, 1994.
37. Hosoi G, Hara J, Okamura T, Osugi Y, Ishihara S, Fukuzawa M, Okada A, Okada S and Tawa A: Low frequency of the p53 gene mutations in neuroblastoma. Cancer 73: 3087-3093, 1994.
38. Keshelava N, Zuo JJ, Chen P, Waidyaratne SN, Luna MC, Gomer CJ, Triche TJ and Reynolds CP: Loss of p53 function confers high-level multidrug resistance in neuroblastoma cell lines. Cancer Res 61: 6185-6193, 2001.
39. Moll UM, LaQuaglia M, Benard J and Riou G: Wild-type p53 protein undergoes cytoplasmic sequestration in undifferentiated neuroblastomas but not in differentiated tumors. Proc Natl Acad Sci USA 92: 4407-4411, 1995.
40. Aloyz RS, Bamji SX, Pozniak CD, Toma JG, Atwal J, Kaplan DR and Miller FD: p53 is essential for developmental neuron death as regulated by the TrkA and p75 neurotrophin receptors. J Cell Biol 143: 1691-1703, 1998.
41. Nakagawa T, Takahashi M, Ozaki T, Watanabe Ki K, Todo S, Mizuguchi H, Hayakawa T and Nakagawara A: Autoinhibitory regulation of p73 by Delta Np73 to modulate cell survival and death through a p73-specific target element within the Delta Np73 promoter. Mol Cell Biol 22: 2575-2585, 2002.
42. Takahashi M, Seki N, Ozaki T, Kato M, Kuno T, Nakagawa T, Watanabe K, Miyazaki K, Ohira M, Hayashi S, Hosoda M, Tokita H, Mizuguchi H, Hayakawa T, Todo S and Nakagawara A: Identification of the p33(*ING1*)-regulated genes that include cyclin B1 and proto-oncogene DEK by using cDNA microarray in a mouse mammary epithelial cell line NMuMG. Cancer Res 62: 2203-2209, 2002.

THE JOURNAL OF BIOLOGICAL CHEMISTRY
Vol. 279, No. 24, Issue of June 11, pp. 25549–25561, 2004
Printed in U.S.A.

Polo-like Kinase 1 (Plk1) Inhibits p53 Function by Physical Interaction and Phosphorylation*

Received for publication, December 26, 2003, and in revised form, March 11, 2004
Published, JBC Papers in Press, March 15, 2004, DOI 10.1074/jbc.M314182200

Kiyohiro Ando‡§¶, Toshinori Ozaki‡¶, Hideki Yamamoto‡, Kazushige Furuya‡, Mitsuchika Hosoda‡, Syunji Hayashi‡, Masahiro Fukuzawa§, and Akira Nakagawara‡‖

From the ‡Division of Biochemistry, Chiba Cancer Center Research Institute, Chiba 260-8717, Japan and the §First Department of Surgery, Nihon University School of Medicine, Tokyo 173-8610, Japan

Polo-like kinase 1 (Plk1) has an important role in the regulation of M phase of the cell cycle. In addition to its cell cycle-regulatory function, Plk1 has a potential role in tumorigenesis. Here we found for the first time that Plk1 physically binds to the tumor suppressor p53 in mammalian cultured cells, and inhibits its transactivation activity as well as its pro-apoptotic function. During the cisplatin-induced apoptosis in human neuroblastoma SH-SY5Y cells, the expression level of Plk1 was significantly decreased both at mRNA and protein levels, whereas cisplatin treatment caused a remarkable stabilization of p53. Systematic immunoprecipitation analyses using a series of deletion mutants of p53 revealed that a sequence-specific DNA-binding region of p53 is required and sufficient for the physical interaction with Plk1. The ectopically overexpressed Plk1 was co-localized with the endogenous p53 in mammalian cell nucleus, as shown by confocal laser microscopy. Expression of exogenous Plk1 and p53 in p53-deficient lung carcinoma H1299 cells greatly decreased the p53-mediated transcription from the p53-responsive $p21^{WAF1}$, *MDM2*, and *BAX* promoters, whereas the kinase-deficient mutant form of Plk1 failed to reduce the transcriptional activity of p53. Consistent with the luciferase reporter analysis, Plk1 had an ability to block the p53-dependent induction of the endogenous $p21^{WAF1}$. In addition, Plk1 inhibited the pro-apoptotic function of p53 in H1299 cells. Intriguingly, Plk1-mediated repression of p53 was attenuated with ATM. Thus, our present findings strongly suggest that p53 is a critical target of Plk1, and its function is abrogated through the physical interaction with Plk1.

The polo-like kinases (Plks)[1] are structurally and functionally related to the *Drosophila* polo serine/threonine (Ser/Thr) kinase (1), and are evolutionarily well conserved from yeast to mammals. A high degree of amino acid sequence similarity is detected within a catalytic domain and a unique noncatalytic domain (termed the polo-box) located at the NH_2- and COOH-terminal region, respectively (2). It has been shown that the polo-box is critical for the correct subcellular localization of Plks (3, 4), and the COOH-terminal region containing the polo-box serves to regulate its kinase activity (5). A growing body of evidence obtained in various experimental systems suggests that Plks play an important role in the regulation of a variety of M-phase-specific events including entry into and exit from mitosis (1, 6–8). In addition to their critical role during the G_2/M transition, Plks might be also required for G_1/S phase transition (9, 10).

In mammalian cells, there exist at least three Plk family members including Plk1, Plk2, and Plk3. Plk1 (also referred to as Plk) has been identified as a serine/threonine kinase that displays an extensive amino acid sequence homology to *Drosophila* polo (2, 9, 11–13), whereas Plk2 (alternatively named Snk) and Plk3 (alternatively termed as proliferation related kinase, Prk) have been originally shown to be transcriptionally induced in response to mitogens (14, 15). In mammalian cultured cells, the amounts of Plk1 mRNA and protein are regulated in a cell cycle-dependent manner, rising from a very low level in G_1 phase to a maximal level during G_2/M phase (11, 12). The kinase activity of Plk1 is regulated by its phosphorylation and peaks at M phase (16–18). Recently, it has been shown that the kinase activity of Plk1 is inhibited in response to DNA damage in mammalian cultured cells and this inhibition occurs in an ATM-dependent manner (19, 20). Plk1 phosphorylates various substrate proteins including cyclin B1 and Cdc25C. At the onset of mitosis, Plk1 phosphorylated cyclin B1 and promoted rapid nuclear translocation of an active Cdc2-cyclin B1 complex (21, 22). In addition, Toyoshima-Morimoto *et al.* (23) has found that, during G_2/M phase, Plk1 is capable of phosphorylating Cdc25C, which dephosphorylates and directly activates the Cdc2-cyclin B1 complex, and regulating the nuclear entry of Cdc25C. In contrast to Plk1, the expression level of Plk3 remains constant during the cell cycle progression and its kinase activity peaks during late S and G_2 phase (24, 25). Xie *et al.* (26) found that the kinase activity of Plk3 is rapidly increased in response to DNA damage in an ATM-dependent fashion.

In addition to the potential cell cycle-regulatory role, Plk1 has been implicated in the genesis and/or progression of tumors. *Plk1* was overexpressed in rapidly proliferating cells as well as various human primary tumors (27), suggesting that the expression level of *Plk1* is tightly linked to proliferation and could be used as a negative prognostic indicator for various

* This work was supported in part by a grant-in-aid from the Ministry of Health and Welfare for a New 10-Year Strategy for Cancer Control, a grant-in-aid for Scientific Research on Priority Areas, a grant-in-aid for Scientific Research (B) from the Ministry of Education, Science, Sports and Culture, Japan, and the Hisamitsu Pharmaceutical Company. The costs of publication of this article were defrayed in part by the payment of page charges. This article must therefore be hereby marked "*advertisement*" in accordance with 18 U.S.C. Section 1734 solely to indicate this fact.

¶ Both authors contributed equally to this work.
‖ To whom correspondence should be addressed: Division of Biochemistry, Chiba Cancer Center Research Institute, 666-2 Nitona, Chuoh-ku, Chiba 260-8717, Japan. Tel.: 81-43-264-5431; Fax: 81-43-265-4459; E-mail: akiranak@chiba-ccri.chuo.chiba.jp.

[1] The abbreviations used are: Plk, polo-like kinase; ATM, ataxia telangiectasia mutated; GFP, green fluorescence protein; GST, glutathione *S*-transferase; NLS, nuclear localization signal; NMS, normal mouse serum; PBS, phosphate-buffered saline; TBS, Tris-buffered saline; TK, thymidine kinase; RT, reverse transcriptase.

tumors (28–30). Consistent with these observations, constitutive overexpression of Plk1 in NIH3T3 cells resulted in the oncogenic focus formation and induction of tumor growth in nude mice (10). Down-regulation of the endogenous *Plk1* by using several antisense oligonucleotides targeted to *Plk1* induced growth inhibition in certain cancerous cells (31). Additionally, treatment of the cells with small interfering RNA targeted against *Plk1* caused the cell cycle arrest and apoptosis (32, 33). Of note, Liu and Erikson (33) reported that the tumor suppressor p53 might be involved in the Plk1 depletion-induced apoptosis. Recently, Plk1 has also been reported to have an ability to phosphorylate p53 *in vitro*, however, it is still unknown whether there exists a functional association between Plk1 and p53 (26). In sharp contrast to *Plk1*, the expression level of *Plk3* was significantly down-regulated in several human primary tumors including lung carcinomas and head and neck squamous cell carcinomas, as compared with their corresponding normal tissues (34, 35). Overexpression of Plk3 in mammalian cultured cells inhibited proliferation and induced apoptosis (36). Furthermore, it has been demonstrated that Plk3 physically interacts with p53 and phosphorylates the Ser^{20} of p53, which might result in the enhancement of its activity. These suggest that Plk1 and Plk3 play a differential role in regulating cell proliferation and oncogenesis, and that p53 participates in Plk3-dependent growth inhibition and/or apoptosis (25, 26, 36, 37).

In the present study, we examined the physical and functional interaction between Plk1 and p53. We found that Plk1 binds to the sequence-specific DNA-binding domain of p53, and inhibits the p53-dependent transcriptional activation as well as pro-apoptotic function. Intriguingly, overexpression of ATM abrogated the Plk1-mediated inhibitory effect on p53. These results suggest that the Plk1-mediated negative regulation of p53 might be a fundamental mechanism for the Plk1-induced oncogenesis.

EXPERIMENTAL PROCEDURES

Tumor Samples—Surgically resected tumor tissues including three lung adenocarcinomas, two gastric adenocarcinomas, one uterus carcinoma, two bladder carcinomas, and their corresponding normal tissues used in this study were obtained as frozen specimens from the Tissue Bank in Chiba Cancer Center Hospital (Chiba, Japan). Six hepatoblastomas and their matched normal tissues were provided by the Japanese Study Group for Pediatric Liver Tumor.

Cell Culture—African green monkey kidney COS7 cells were maintained in Dulbecco's modified Eagle's medium supplemented with 10% heat-inactivated fetal bovine serum (Invitrogen) and penicillin (100 IU/ml)/streptomycin (100 μg/ml). Human neuroblastoma SH-SY5Y cells and human lung carcinoma H1299 cells were grown in RPMI 1640 medium containing 10% heat-inactivated fetal bovine serum and antibiotic mixture. Cultures were maintained at 37 °C in a water-saturated atmosphere of 5% CO_2 in air.

Transfection—COS7 cells were transfected with the indicated expression plasmids using FuGENE 6 transfection reagent (Roche Applied Science) in a 6-cm diameter culture dish in accordance with the manufacturer's specifications. Transfection of H1299 cells was conducted by lipofection with LipofectAMINE transfection reagent (Invitrogen) in a 12-well plate according to the manufacturer's instructions.

RT-PCR—Total RNA was prepared from SH-SY5Y cells exposed to cisplatin by using the RNeasy Mini Kit (Qiagen Inc., Valencia, CA) according to the manufacturer's protocol, and subjected to synthesis of the first strand cDNA with random primers and a SuperScript II reverse transcriptase (Invitrogen) at 42 °C for 1 h. When the reaction was complete, the cDNA was amplified in a final volume of 15 μl of reaction mixture containing 100 μM of each deoxynucleoside triphosphate, 1× PCR buffer, 1 μM of each primer, and 0.2 units of rTaq DNA polymerase (Takara, Ohtsu, Japan). The primers for *p53* amplification were 5′-ATTTGATGCTGTCCCCGGACGATATTGAAC-3′ and 5′-ACCCTTTTTGGACTTCAGGTGGCTGGAGTG-3′. The primers for $p21^{WAF1}$ amplification were 5′-ATGAAATTCACCCCCTTTCC-3′ and 5′-CCCTAGGCTGTGCTCACTTC-3′. The primers for *Plk1* amplification were 5′-ATCACCTGCCTGACCATTCCACCAAGG-3′ and 5′-AATTGCGGAAATATTTAAGGAGGGTGATCT-3′. The primers for *Plk3* amplification were 5′-GCGCGAGAAGATCCTAAATG-3′ and 5′-GATCTGCCGCAGGTAGTAGC-3′. The primers for *GAPDH* amplification were 5′-ACCTGACCTGCCGTCTAGAA-3′ and 5′-TCCACCACCCTGTTGCTGTA-3′. The PCR-amplified products were separated by electrophoresis on a 1.5% agarose gel and visualized by ethidium bromide post-staining.

Generation of FLAG-tagged Expression Constructs—The FLAG-tagged human *Plk1* construct was generated by PCR amplification using the cDNA derived from primary hepatoblastoma as a template. The forward and reverse primers used in the PCR were 5′-CCGCTCGAGAGTGCTGCAGTGACTGCAGGGAAG-3′ and 5′-CTAGTCTAGATTAGGAGGCCTTGAGACGGTTGCT-3′. The underlined nucleotides represent the XhoI restriction sites in the forward primer and the XbaI restriction site in the reverse primer. The PCR product was subcloned into pGEM-T Easy (Promega Corp., Madison, WI), and its nucleotide sequence was verified by automated dideoxy terminator cycle sequencing. The PCR product was digested with XhoI and XbaI, and inserted between the XhoI to XbaI sites in the pcDNA3-FLAG expression plasmid in-frame to the downstream of the FLAG tag to give pcDNA3-FLAG-*Plk1*.

Construction of the Deletion Mutants of p53 and Plk1—The *p53* deletion mutants, *p53*-(1–359), *p53*-(1–292), and *p53*-(1–101) were generated by using the forward primer 5′-CCCAAGCTTGGGATGGAGGAGCCGCAGTCAGATCCTAGCGTC-3′ (1F) in combination with the reverse primers 5′-CCGGAATTCCGGTCATGGCTCCTTCCCAGCCTGGGCATCCTT-3′ (359R), 5′-CCGGAATTCCGGTCATTTCTTGCGGAGATTCTCTTCCTCTGT-3′ (292R) and 5′-CCGGAATTCCGGTCATTTCTGGGAAGGGACAGAAGATGACA-3′ (101R), respectively. *p53*-(102–393) was amplified by using the forward primer 5′-CCCAAGCTTGGGATGACCTACCAGGGCAGCTACGGTTTCCGTCT-3′ (102F) and the reverse primer 5′-CCGGAATTCCGGTCAGTCTGAGTCAGGCCCTTCTGTCTTGAACAT-3′ (393R). Each of the forward and reverse primers contained the HindIII and EcoRI restriction sites to facilitate the subsequent cloning step. Underlined nucleotides in the oligonucleotides listed above were HindIII or EcoRI sites. Amplified fragments were digested with HindIII and EcoRI, and subcloned directly into the identical restriction sites of pcDNA3 to give pcDNA3-*p53*-(1–359), pcDNA3-*p53*-(1–292), pcDNA3-*p53*-(1–101), and pcDNA3-*p53*-(102–393). All of the constructs were confirmed by sequence analysis. For the construction of the deletion mutants of Plk1, pcDNA3-FLAG-*Plk1* was digested with BamHI, BamHI and BstXI, or BamHI and NcoI. A restriction fragment encoding amino acid residues 1–401, 1–329, or 1–98 was purified from agarose gels, filled in the overhangs with Klenow, and then inserted in-frame into the enzymatically modified BamHI and XhoI sites of the pcDNA3-FLAG expression plasmid to give pcDNA3-FLAG-*Plk1*-(1–401), pcDNA3-FLAG-*Plk1*-(1–329), or pcDNA3-FLAG-*Plk1*-(1–98), respectively. DNA sequencing confirmed the authenticity of the expression plasmids prior to transfection.

Construction of the Kinase-deficient Mutant Form of Plk1—The K82M mutation was introduced into wild-type Plk1 by the PCR-based strategy using *PfuUltra*™ High Fidelity DNA polymerase (Stratagene, La Jolla, CA) according to the manufacturer's instructions. The following oligonucleotides were used: 5′-ATGATTGTGCCTAAGTCTCTGCTGCTCAAGCCGCA-3′ (underlined segment encodes Met at amino acid position 82) and 5′-GCCCGCGAACACCTCCTTGGTGTCCGCGTCCGAGA-3′. Nucleic acid sequencing was performed to verify the presence of the desired mutation and absence of random mutations. The amplified fragment that contains the K82M mutation was then digested with HindIII and NcoI, gel-purified, and ligated with the NcoI/XbaI restriction fragment containing the 3′-portion of the wild-type *Plk1* cDNA. The resulting entire cDNA encoding the full-length Plk1 carrying the amino acid substitution at position 82 was inserted in-frame into the HindIII and XbaI sites of the pcDNA3-FLAG expression plasmid to give pcDNA3-FLAG-*Plk1*(K82M).

Construction of the Expression Plasmid for Antisense Plk1—A full-length human *Plk1* cDNA was ligated into the pcDNA3 expression plasmid in a reverse orientation to give As-*Plk1*, and the product was evaluated by restriction digestion. To assess the effect of As-*Plk1* on the endogenous Plk1, whole cell lysates prepared from H1299 cells transfected with As-*Plk1* were analyzed for Plk1 by immunoblotting.

GST Pull-down Assay—Whole cell lysates prepared from COS7 cells expressing FLAG-Plk1 were incubated with 1 μg of GST or GST-p53 (Santa Cruz Biotechnologies, Santa Cruz, CA) immobilized on glutathione-Sepharose beads for 2 h at 4 °C. The beads were washed extensively with NETN buffer (50 mM Tris-Cl, pH 7.5, 150 mM NaCl, 0.1% Nonidet P-40, and 1 mM EDTA) containing 1 mM phenylmethylsulfonyl fluoride. The bound proteins were eluted with 2× SDS sample buffer by boiling

for 5 min, and separated by 10% SDS-polyacrylamide gel electrophoresis followed by immunoblotting.

Immunofluorescent Labeling and Confocal Microscopy—COS7 cells, cultured onto glass coverslips, were transiently transfected with the expression plasmid for FLAG-Plk1. Transfected cells were washed twice with 1× PBS and then fixed with 1× PBS containing 3.7% formaldehyde for 30 min at room temperature. After washing with 1× PBS, cells were permeabilized with 0.2% Triton X-100 for 5 min at room temperature and blocked for 1 h in 1× PBS containing 3% bovine serum albumin. Cells were then incubated with polyclonal anti-p53 antibody (Cell Signaling Technology, Inc., Beverly, MA) and monoclonal anti-FLAG antibody (M2, Sigma) for 1 h at room temperature. After incubation with primary antibodies, cells were washed twice with 1× PBS and incubated with fluorescein isothiocyanate- or rhodamine-conjugated secondary antibodies (Invitrogen) diluted 1:200 for 1 h at room temperature. Cell nuclei were stained with 4,6-diamidino-2-phenylindole at a final concentration of 1 μg/ml (Sigma). Cells were finally washed with 1× PBS, the coverslips were removed from the dishes, mounted onto slides, and observed under Fluoview laser scanning confocal microscope (Olympus, Tokyo, Japan).

Western Blot Analysis—Cells were transfected with the indicated combinations of the expression plasmids. Forty-eight hours after transfection, cells were extracted directly with the lysis buffer containing 25 mM Tris-HCl, pH 8.0, 137 mM NaCl, 2.7 mM KCl, 1% Triton X-100, 1 mM phenylmethylsulfonyl fluoride and protease inhibitor mixture (Sigma) and the whole cell lysates were sonicated for 10 s followed by centrifugation at 15,000 rpm for 10 min at 4 °C to remove insoluble materials. The protein concentrations were determined using the Bradford protein assay according to the instructions of the vendor (Bio-Rad). Equal amounts of the whole cell lysates (50 μg of protein) were boiled in an SDS sample buffer consisting of 62.5 mM Tris-HCl, pH 6.8, 2% SDS, 2% β-mercaptoethanol, and 0.01% bromphenol blue and subjected to 10% SDS-polyacrylamide gel electrophoresis under reducing conditions and then electrotransferred onto Immobilon-P membranes (Millipore, Bedford, MA) at room temperature for 1 h. The membranes were blocked with TBS-T (50 mM Tris-Cl, pH 7.6, 100 mM NaCl, and 0.1% Tween 20) containing 5% nonfat dry milk at room temperature for 1 h, and subsequently incubated for 1 h with monoclonal anti-Plk1 (PL2 and PL6, Zymed Laboratories, Inc., San Francisco, CA), monoclonal anti-p53 (DO-1, Oncogene Research Products, Cambridge, MA), monoclonal anti-FLAG antibody (M2, Sigma), monoclonal anti-Plk3 antibody (B37–2, BD Pharmingen), polyclonal antibody specific for p53 phosphorylated at Ser^{15} (Cell Signaling, Beverly, MA), polyclonal anti-$p21^{WAF1}$ antibody (H-164, Santa Cruz Biotechnologies), or polyclonal anti-actin antibody (20–33, Sigma) in TBS-T, followed by an incubation with horseradish peroxidase-conjugated goat anti-mouse or anti-rabbit secondary antibody (Jackson ImmunoResearch Laboratories, West Grove, PA) diluted at 1:2,000 for 1 h at room temperature. The membranes were washed extensively with TBS-T and protein bands were visualized by enhanced chemiluminescence (ECL) according to the manufacturer's instructions (Amersham Biosciences).

Subcellular Fractionation—Cells were fractionated into cytosolic and nuclear fractions as described previously (38). Briefly, cells were washed twice with ice-cold 1× PBS and lysed in lysis buffer containing 10 mM Tris-HCl, pH 7.5, 1 mM EDTA, 0.5% Nonidet P-40, and a protease inhibitor mixture (Sigma) for 30 min at 4 °C. Cell lysates were centrifuged at 15,000 × *g* for 10 min to collect the soluble fraction as cytosolic extracts. Insoluble materials were washed with the lysis buffer and further dissolved in 1× SDS sample buffer to collect the nuclear fraction. The nuclear and cytoplasmic fractions were subjected to immunoblot analysis using the anti-FLAG, monoclonal anti-lamin B (Ab-1, Oncogene Research Products), or monoclonal anti-Ras (RASK-3, Seikagaku Co., Tokyo, Japan) antibody.

Immunoprecipitation and Western Blot Analysis—For the immunoprecipitation of Plk1 and p53, COS7 cells were transiently transfected with 2 μg of the expression plasmid for FLAG-Plk1 using FuGENE 6 transfection reagent. Forty-eight hours post-transfection, cells were harvested and lysed by incubation with mixing in 400 μl of the EBC buffer (50 mM Tris-HCl, pH 7.5, 120 mM NaCl, 0.5% Nonidet P-40, and 1 mM phenylmethylsulfonyl fluoride) at 4 °C for 30 min. Whole cell lysates were then subjected to centrifugation at 15,000 × *g* for 20 min at 4 °C to remove insoluble materials. Equal amounts of whole cell lysates were precleared with 30 μl of a 50% slurry of protein A-Sepharose (Amersham Biosciences). After centrifugation, the supernatant was incubated with the normal mouse serum (NMS), monoclonal anti-FLAG, or monoclonal anti-p53 antibody at 4 °C for 2 h. The immunocomplexes were precipitated with the protein A-Sepharose beads at 4 °C for 30 min, which were then pelleted by centrifugation at 15,000 × *g* for 5 min. The precipitates were washed with the lysis buffer three times at 4 °C, resuspended in 30 μl of the SDS sample buffer, and treated at 100 °C for 5 min. Proteins were then resolved by 10% SDS-polyacrylamide gel electrophoresis, and transferred onto the Immobilon-P membranes. The protein complex was detected by Western blot analysis using the monoclonal anti-FLAG or monoclonal anti-p53 antibodies.

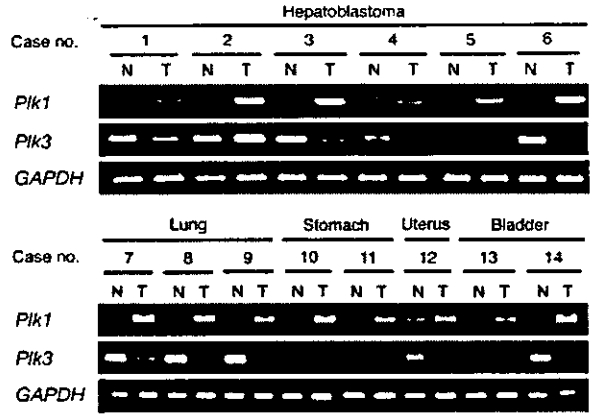

FIG. 1. **Expression of *Plk1* and *Plk3* mRNA in various human primary tumors and their corresponding normal tissues.** Total RNA (5 μg) prepared from the indicated tumor (*T*)-normal (*N*) paired samples was subjected to RT-PCR analysis for *Plk1* and *Plk3* mRNA expression using the specific primers as shown under "Experimental Procedures." The PCR-amplified products were analyzed by 1.5% agarose gel electrophoresis and visualized by ethidium bromide staining. Amplification of *GAPDH* was used as an internal control.

Luciferase Reporter Assays—p53-deficient H1299 cells were seeded in a 12-well tissue culture dish at a density of 5×10^4 cells/well. Cells were transfected with 100 ng of the p53-responsive luciferase reporter plasmid (*p21*, *MDM2*, or *BAX*), 10 ng of pRL-TK *Renilla* luciferase cDNA, and 25 ng of the expression plasmid for p53 together with or without increasing amounts of FLAG-Plk1 expression plasmid. The total amount of DNA was kept constant (510 ng) with pcDNA3 (Invitrogen) per transfection. Forty-eight hours post-transfection, transfected cells were washed twice with 1× PBS, and resuspended in passive lysis buffer (Promega Corp.). Both firefly and *Renilla* luciferase activities were assayed with the dual-luciferase reporter assay system (Promega Corp.) according to the manufacturer's instructions. The fluorescent light emission was determined by TD-20 luminometer (Turner Design, Sunnylvale, CA). The firefly luminescence signal was normalized based on the *Renilla* luminescence signal. The results were obtained from at least three sets of transfection and were presented as the mean ± S.D.

Cell Survival Assays—Cell viability was determined by a modified 3-(4,5-dimethylthiazol-2-yl)-2,5-diphenyltetrazolium bromide (MTT) assay. In brief, SH-SY5Y cells were seeded in 96-well microtiter plates (5×10^3 cell/well) with 100 μl of complete medium and allowed to attach. The next day, the medium were changed and cells were treated with cisplatin for 24 h. For the MTT assay, 10 μl of MTT solution was added to each well for 3 h at 37 °C. The absorbance readings for each well were carried out at 570 nm using the microplate reader (model 450, Bio-Rad).

Apoptotic Analysis—H1299 cells were transfected with a constant amount of the expression plasmid for green fluorescence protein (GFP) and p53 expression plasmid together with or without the expression plasmid encoding FLAG-Plk1. Forty-eight hours after transfection, transfected cells were identified by the presence of green fluorescence. To verify apoptosis, cell nucleus was stained with propidium iodide to reveal nuclear condensation and fragmentation. The number of GFP-positive cells with fragmented nuclei was scored, and presented as a percentage of the total number of fluorescent cells.

RESULTS

Expression of Plk1 and Plk3 in Paired Tumors and Adjacent Normal Tissues—It has been shown that the expression level of *Plk1* is increased in human tumors of various origins as compared with that of their corresponding normal tissues, suggesting that Plk1 contributes to the genesis and/or progression of tumors (13, 27–29). Recently, we have also identified *Plk1* as

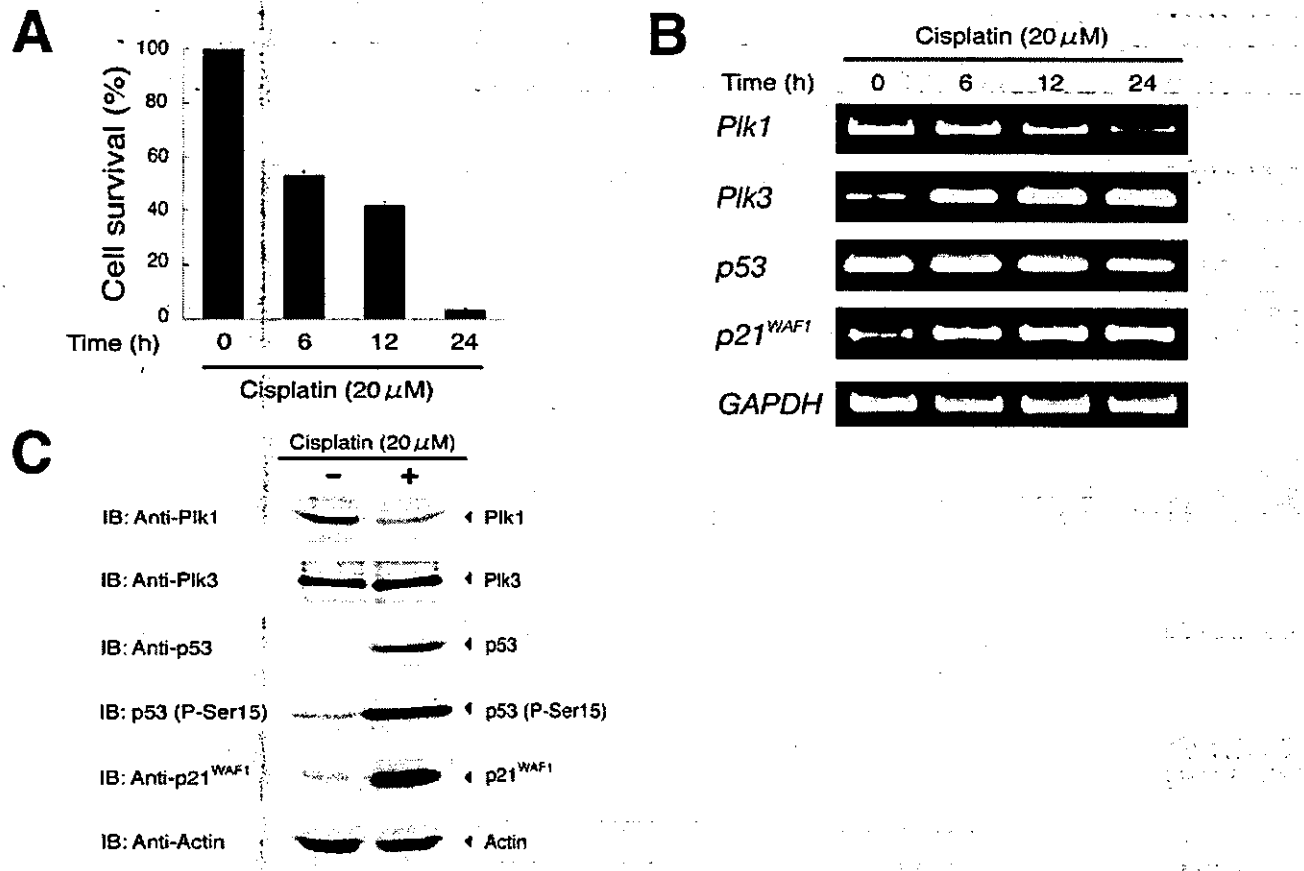

FIG. 2. **Down-regulation of *Plk1* during the cisplatin-induced apoptosis.** *A*, cell survival assays of SH-SY5Y cells treated with cisplatin. SH-SY5Y cells were exposed to cisplatin at a final concentration of 20 μM. At the indicated time periods after treatment with cisplatin, cell viability was determined by MTT assay. Data are presented as the mean ± S.D. of three independent experiments. *B*, RT-PCR analysis. Human neuroblastoma-derived SH-SY5Y cells were treated with or without cisplatin at a final concentration of 20 μM. At the indicated time periods after treatment with cisplatin, total RNA was prepared and subjected to RT-PCR analysis for the expression of *Plk1* (*1st panel*), *Plk3* (*2nd panel*), *p53* (*3rd panel*), and *p21*^{WAF1} (*4th panel*). Amplification of *GAPDH* serves as an internal control (*5th panel*). The PCR products were resolved in 1.5% agarose gels and visualized by ethidium bromide staining. *C*, Western blot analysis. Whole cell lysates were prepared from SH-SY5Y cells exposed to cisplatin for 24 h (at a final concentration of 20 μM) or left untreated and immunoblotted against anti-Plk1 (*1st panel*), anti-Plk3 (*2nd panel*), anti-p53 (*3rd panel*), antibody specific for p53 phosphorylated at Ser^{15} (*4th panel*), or with the anti-p21^{WAF1} antibody (*5th panel*). Immunoblotting for actin is shown as control for protein loading (*6th panel*).

one of the genes whose expression level is markedly elevated in human hepatoblastomas.[2] In contrast, *Plk3* expression is down-regulated in certain human tumors including lung carcinomas and head and neck squamous cell carcinomas (34, 35). To confirm the differential expression of both *Plk1* and *Plk3* in the same tissue samples, we examined their expression patterns among the indicated various paired cancer-normal tissues by RT-PCR. The levels of *GAPDH* mRNA were comparable between these paired samples. Consistent with the previous results, without exceptions, the expression levels of *Plk1* mRNA were significantly higher in cancerous tissues than those of their adjacent normal tissues (Fig. 1). On the other hand, *Plk3* was expressed at low levels in all the lung, uterus, and bladder carcinomas that we examined, as compared with their corresponding normal tissues, whereas a significant decrease in *Plk3* expression level in tumor tissues was undetectable in 2 of 6 hepatoblastomas and in 1 of 2 gastric carcinomas (Fig. 1). Thus, deregulated overexpression of *Plk1* is detected in all various types of tumors, whereas down-regulation of *Plk3* expression may be restricted to certain tumors.

[2] Yamada, S., Ohira, M., Horie, H., Ando, K., Takayasu, H., Suzuki, Y., Sugano, S., Hirata, T., Goto, T., Matsunaga, T., Hiyama, E., Hayashi, Y., Ando, H., Suita, S., Kaneko, M., Sakaki, F., Hashizume, K., Ohnuma, N., and Nakagawara, A. (2004) *Oncogene*, in press.

Cisplatin Treatment Induces Down-regulation of Plk1 in Association with Up-regulation of p53 in SH-SY5Y Cells—To analyze whether Plk1 expression could be modulated during the cisplatin-induced apoptosis, whole cell lysates and total RNA were prepared from human neuroblastoma-derived SH-SY5Y cells after treatment with or without cisplatin, and were subjected to immunoblot analysis and RT-PCR, respectively. In accordance with our previous observations (39), cells underwent apoptosis in a time-dependent manner as measured by the cell survival assay (Fig. 2*A*), and a remarkable stabilization of p53 at the protein level was detected after treating the cells with cisplatin, accompanied with a significant up-regulation of p21^{WAF1} both at protein and mRNA levels (Fig. 2, *B* and *C*). In addition to the increase in the level of total p53, the phosphorylation of p53 at Ser^{15} was dramatically enhanced in cells exposed to cisplatin, whereas that of p53 at Ser^{20} was undetectable (data not shown). Intriguingly, cisplatin treatment markedly reduced the expression level of *Plk1* mRNA and protein (Fig. 2, *B* and *C*), suggesting that there exists an inverse relationship between the expression levels of p53 and Plk1 during DNA damage-induced apoptosis. Thus, Plk1 may play an important role in the p53 pathway. On the other hand, cisplatin treatment resulted in a significant up-regulation of *Plk3* mRNA expression in a time-dependent manner, however,

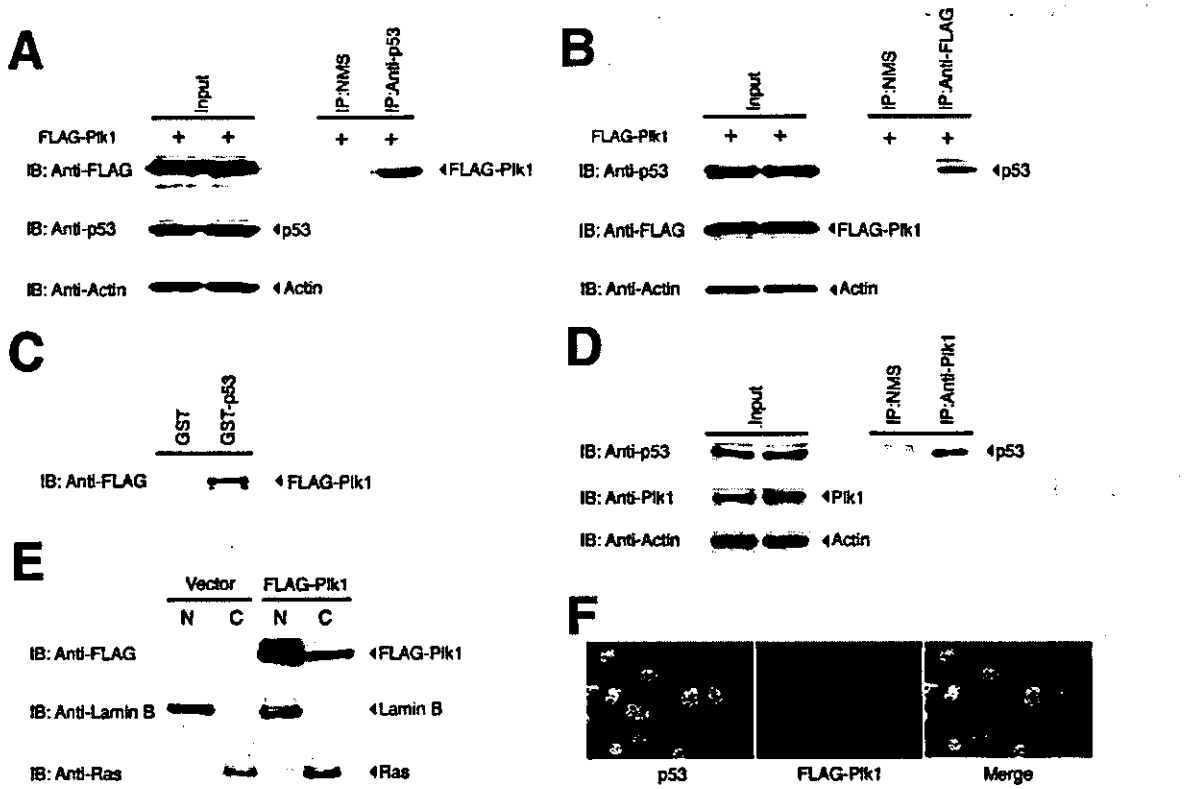

FIG. 3. **Co-immunoprecipitation and nuclear co-localization of Plk1 and p53.** *A*, complex formation between Plk1 and p53 in mammalian cultured cells. COS7 cells were transiently transfected with the expression plasmid for FLAG-tagged Plk1. Forty-eight hours after transfection, whole cell lysates were prepared and immunoprecipitated (*IP*) with NMS or with monoclonal anti-p53 antibodies. The immunocomplexes were resolved by 10% SDS-polyacrylamide gel electrophoresis and immunoblotted (*IB*) with monoclonal anti-FLAG antibody. Whole cell lysates were immunoblotted with monoclonal anti-p53, or with monoclonal anti-FLAG antibody to show the expression of endogenous p53, or FLAG-Plk1, respectively. The p53 blot was reprobed for actin to ensure equal loading. *B*, a similar immunoprecipitation assay was performed with NMS or monoclonal anti-FLAG antibody, followed by immunoblotting with monoclonal anti-p53 antibody. Whole cell lysates were monitored on immunoblot for the expression of endogenous p53 or FLAG-Plk1. The p53 blot was reprobed for actin to ensure equal loading. *C*, GST pull-down assay. Whole cell lysates prepared from COS7 cells expressing FLAG-Plk1 were incubated with GST or GST-p53 immobilized on glutathione-Sepharose beads. The bound proteins were separated by 10% SDS-polyacrylamide gel electrophoresis, and subjected to immunoblotting with the anti-FLAG antibody. *D*, association between endogenous p53 and Plk1. Cell lysates prepared from U2OS cells were immunoprecipitated with NMS or with monoclonal anti-Plk1 antibody, and the anti-Plk1 immunoprecipitates were immunoblotted with monoclonal anti-p53 antibody. *E*, subcellular localization of Plk1. COS7 cells were transiently transfected with the expression plasmid encoding FLAG-Plk1. Forty-eight hours after transfection, cells were fractionated into nuclear (*N*) and cytosolic (*C*) fractions as described under "Experimental Procedures." Equal amounts of each fraction were resolved by 10% SDS-polyacrylamide gel electrophoresis and immunoblotted with monoclonal anti-FLAG antibody (*top panel*). These extracts were also immunoblotted with monoclonal antibody specific for lamin B (*middle panel*) or Ras (RASK-3) (*bottom panel*) to show the validity of our fractionation technique. *F*, nuclear co-localization of Plk1 and p53. COS7 cells were transiently transfected with the FLAG-Plk1 expression plasmid. Following transfection, cells were fixed and incubated with polyclonal anti-p53 and monoclonal anti-FLAG antibodies that were revealed by fluorescein isothiocyanate-conjugated anti-rabbit IgG (*green*) and rhodamine-conjugated anti-mouse IgG (*red*), respectively. Merge analysis (*yellow*) showed the nuclear co-localization of Plk1 and p53.

the amount of Plk3 protein remained constant, regardless of cisplatin treatment.

Interaction of Plk1 with p53—Recently, it has been shown that Plk3 interacts with p53 and is directly involved in the stress-induced phosphorylation of p53 on the serine 20 residue (25, 26, 36, 37). Of note, Xie *et al.* (26) found that Plk1 is able to phosphorylate p53 *in vitro*, however, its functional significance *in vivo* remains unclear. These observations prompted us to investigate possible interactions between Plk1 and p53. For this purpose, COS7 cells, which express a large amount of endogenous p53 (40), were transiently transfected with the expression plasmid for FLAG-tagged Plk1. Whole cell lysates prepared from the transfected cells were immunoprecipitated with NMS or with a monoclonal anti-p53 antibody, and the immunoprecipitates were analyzed by immunoblotting with a monoclonal anti-FLAG antibody. As shown in Fig. 3*A*, FLAG-Plk1 was co-immunoprecipitated with the endogenous p53, but not present in the control immunoprecipitates obtained with the normal mouse serum. The expression of FLAG-Plk1 and the endogenous p53 was confirmed by immunoblot analysis with the antibody against the FLAG epitope and p53, respectively (Fig. 3*A*). Analysis of the anti-FLAG immunoprecipitates also revealed that p53 is co-immunoprecipitated with FLAG-Plk1 (Fig. 3*B*). To confirm their interaction *in vitro*, GST pull-down experiments were performed using GST fusion full-length human p53. As shown in Fig. 3*C*, mammalian expressed FLAG-Plk1 bound to GST-p53 but not to GST alone. Their interaction was further examined using endogenous materials. Whole cell lysates prepared from U2OS cells that carry wild-type p53 (41) were immunoprecipitated with a monoclonal anti-Plk1 antibody and the anti-Plk1 immunoprecipitates were analyzed for the presence of the endogenous p53. As shown in Fig. 3*D*, the endogenous p53 was co-immunoprecipitated with the endogenous Plk1. Similar results were also obtained in HeLa cells (data not shown). These results clearly demonstrate that Plk1 interacts with p53 in mammalian cultured cells and *in vitro*.

To evaluate the subcellular localization of Plk1, we per-

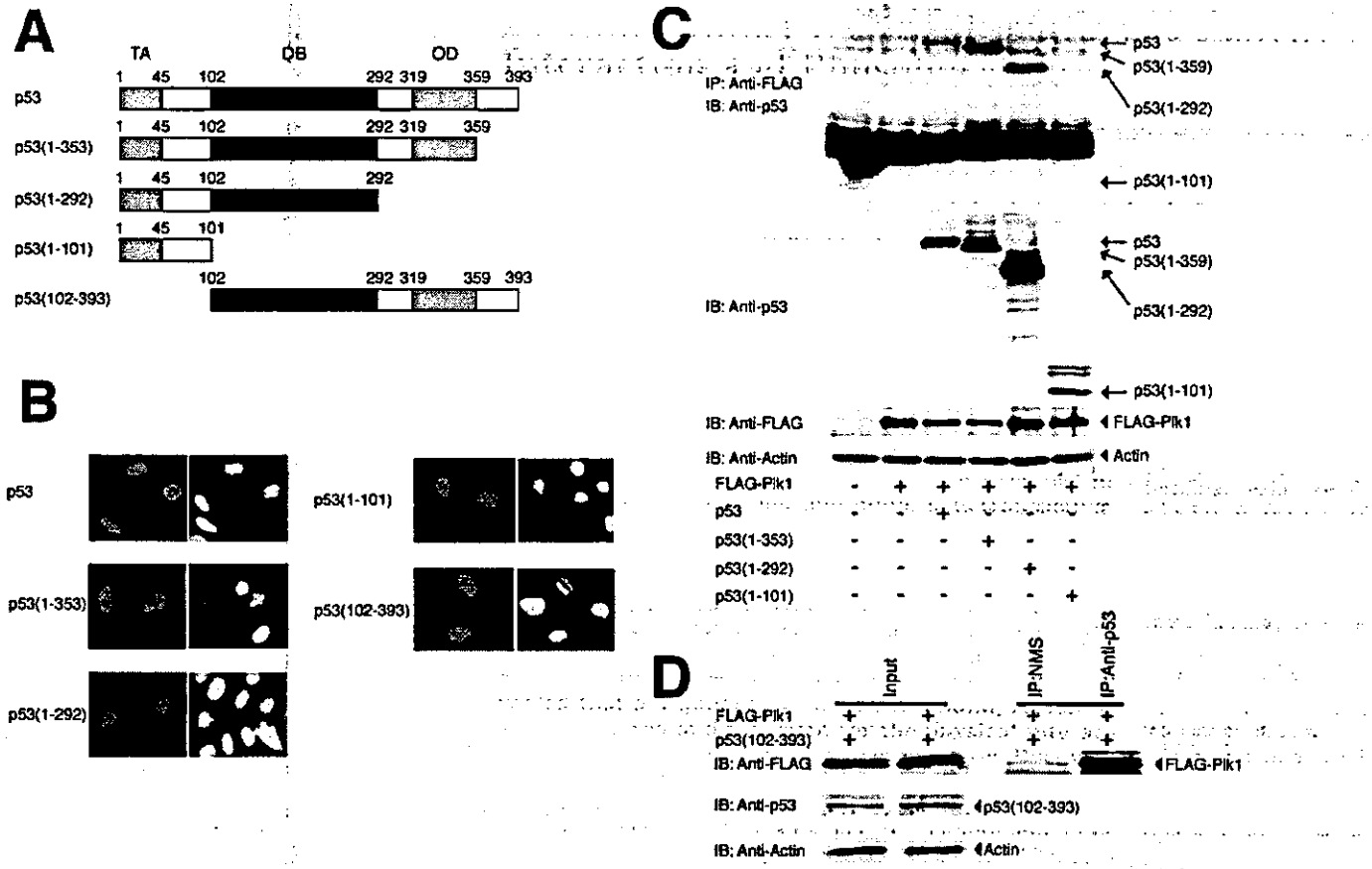

FIG. 4. **DNA-binding domain of p53 is required for interaction with Plk1.** *A*, schematic drawing of full-length p53 and various deletion mutants used in this study. *TA*, transactivation domain; *DB*, sequence-specific DNA-binding domain; *OD*, oligomerization domain. *Numbers* indicate amino acid position. *B*, subcellular localization of various deletion mutants of p53. *p53*-deficient H1299 cells were transiently transfected with the indicated expression plasmids. Forty-eight hours after transfection, cells were fixed and incubated with monoclonal anti-p53 antibody (DO-1 or PAb 421). Cell nuclei were stained with 4,6-diamidino-2-phenylindole (*blue*). Expression of p53 derivatives was visualized with rhodamine-conjugated secondary antibody (*red*). *C* and *D*, Plk1 interacts with the DNA-binding domain of p53. H1299 cells were transiently co-transfected with the indicated combinations of the expression plasmids. Forty-eight hours after transfection, whole cell lysates were prepared and subjected to immunoprecipitation with monoclonal anti-FLAG antibody followed by immunoblotting with monoclonal anti-p53 antibody (*upper panel*). The *lower panels* show the direct immunoblot analyses of whole cell lysates performed with monoclonal anti-p53, monoclonal anti-FLAG, or with polyclonal anti-actin antibody (*C*). Whole cell lysates from H1299 cells overexpressing FLAG-Plk1 and p53-(102–393) were immunoprecipitated with monoclonal anti-p53 antibody (PAb421) or with NMS followed by immunoblotting with monoclonal anti-FLAG antibody. Expression levels of p53-(102–393), FLAG-Plk1, and actin were examined by immunoblotting (*D*).

formed indirect immunofluorescent staining as well as biochemical cell fractionation of the transfected COS7 cells. COS7 cells transfected with the empty plasmid or with the expression plasmid for FLAG-Plk1 were fractionated into cytoplasmic and nuclear fractions for immunoblot analysis of FLAG-Plk1. Ras and lamin B served as markers for the purity of cytoplasmic and nuclear fractions, respectively (Fig. 3*E*, *lower panels*). Consistent with previous observations (10, 22, 42), FLAG-Plk1 was detected both in the cytoplasm and nucleus (Fig. 3*E*, *upper panel*). For immunofluorescent staining, COS7 cells expressing FLAG-Plk1 were fixed and stained with monoclonal anti-FLAG and polyclonal anti-p53 antibodies. As shown in Fig. 3*F*, FLAG-Plk1 localized to both the cytoplasm and nucleus. Merging analysis by confocal microscopy showed that FLAG-Plk1 co-localizes with endogenous p53 in cell nucleus.

The Sequence-specific DNA-binding Region of p53 Is Required for the Interaction with Plk1—To assess regions of p53 involved in the interaction with Plk1, we constructed a series of p53 deletion mutants including p53-(1–359) (lacking an extreme COOH-terminal region), p53-(1–292) (lacking the most COOH-terminal region including an oligomerization domain), p53-(1–101) (retaining only an NH_2-terminal transactivation domain), and p53-(102–393) (lacking an NH_2-terminal transactivation domain) (Fig. 4*A*). We first examined their subcellular localization by indirect immunofluorescent staining. To this end, p53-deficient human lung carcinoma H1299 cells (43) were transiently transfected with each expression plasmid. Forty-eight hours after transfection, cells were fixed and stained with the appropriate monoclonal anti-p53 antibody. As described previously (44, 45), there exist three potential nuclear localization signals (NLS I, II, and III) in the COOH-terminal region of p53, and NLS I alone has an ability to translocate the pyruvate kinase fusion protein to the nucleus. As shown in Fig. 4*B*, wild-type p53 and p53-(102–393), which retain the intact COOH-terminal region, accumulated in the nucleus. In addition, p53-(1–359), which lacks the NLS II and III but retains the NLS I, localized largely in the nucleus. On the other hand, p53-(1–292) and p53-(1–101), which lack three potential NLSs, were detected both in the nucleus and the cytoplasm. We then examined their abilities to interact with Plk1. H1299 cells were transiently co-transfected with the FLAG-Plk1 expression plasmid along with the expression plasmid for wild-type p53, p53-(1–359), p53-(1–292), or p53-(1–101), and the anti-FLAG immunoprecipitates were analyzed for the presence of wild-

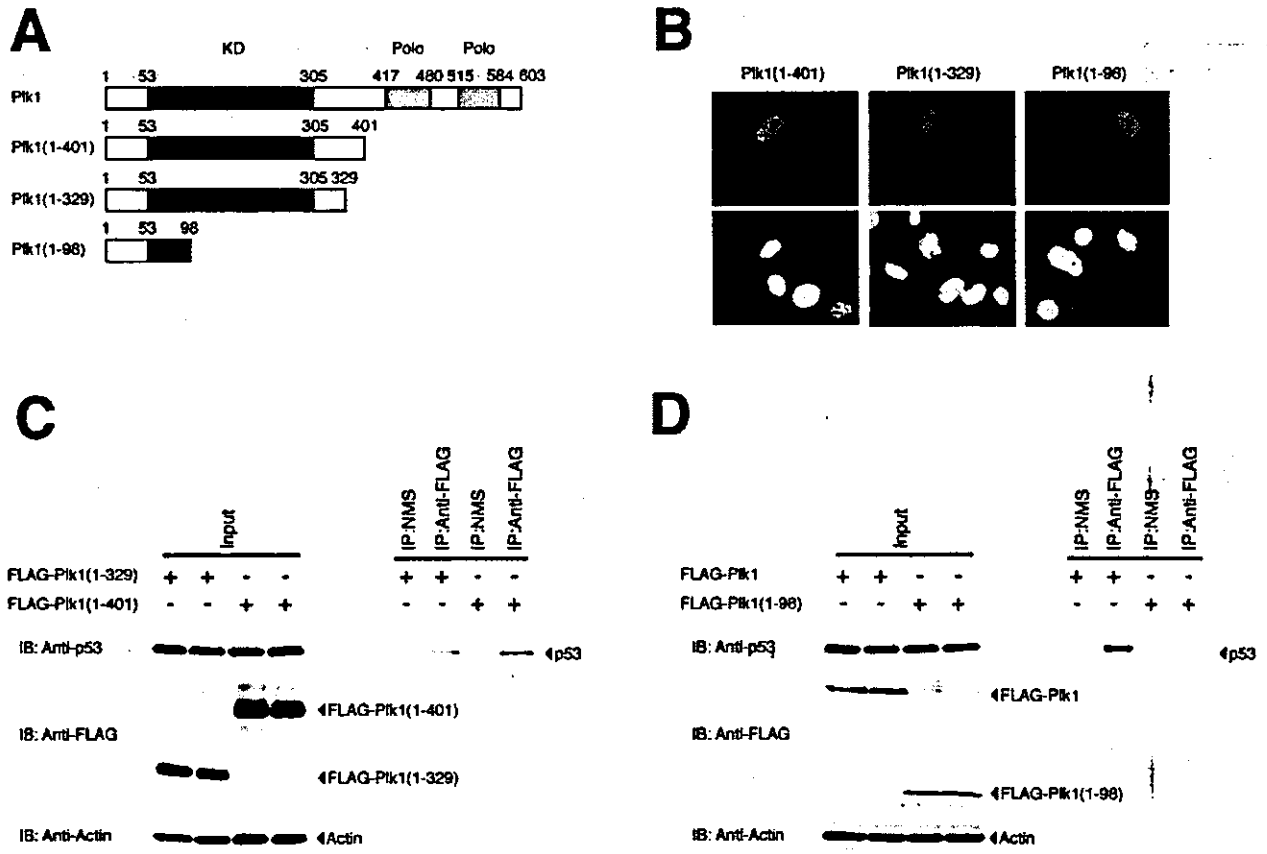

FIG. 5. **Mapping of the region of Plk1 required for interaction with p53.** *A*, schematic representation of Plk1 deletion mutants. *KD*, kinase domain; *Polo*, polo-box. *Numbers* indicate amino acid position. *B*, immunofluorescent studies of Plk1 deletion mutants. Transfected COS7 cells were fixed in 3.7% formaldehyde for 30 min, permeabilized with 0.2% Triton X-100 for 5 min, and blocked in PBS containing 3% bovine serum albumin for 1 h. Cells were then incubated with monoclonal anti-FLAG antibody followed by incubation with rhodamine-conjugated secondary antibody (*red*), and analyzed by confocal microscopy. Cell nuclei were stained with 4,6-diamidino-2-phenylindole (*blue*). *C* and *D*, interaction between various Plk1 deletion mutants and endogenous p53. Whole cell lysates from COS7 cells transfected with the indicated expression plasmids were immunoprecipitated with monoclonal anti-FLAG antibody, and immunoblotted with monoclonal anti-p53 antibody to observe the interaction between Plk1 deletion mutants and p53. Immunoprecipitation with NMS was used as a negative control. Equal amounts of protein derived from cell lysates were immunoblotted with monoclonal anti-p53, monoclonal anti-FLAG, or polyclonal anti-actin antibody.

type p53 and these truncated forms of p53. As shown in Fig. 4*C*, wild-type p53 as well as p53 deletion mutants including p53-(1–359) and p53-(1–292), were detected in the anti-FLAG immunoprecipitates, whereas p53-(1–101) has lost the ability to bind to Plk1, indicating that the extreme COOH-terminal region, the oligomerization domain, and the NH_2-terminal transactivation domain of p53 are not involved in the interaction with Plk1. Similar immunoprecipitation analyses revealed that p53-(102–393) co-precipitates with FLAG-Plk1 (Fig. 4*D*). Thus, the region between amino acid residues 102 and 292 of p53, which includes the sequence-specific DNA-binding domain, appears to be required and sufficient for the interaction with Plk1.

Mapping of the p53-binding Region of Plk1—To map the p53-interacting domain on Plk1, we have constructed the FLAG-tagged Plk1 deletion mutants including Plk1-(1–401), Plk1-(1–329), and Plk1-(1–98) (Fig. 5*A*), and examined their subcellular localization by indirect immunofluorescent staining. As shown in Fig. 5*B*, COS7 cells transfected with each of the expression plasmids for FLAG-tagged Plk1 deletion mutants exhibited intense staining of the nucleus. Inspection of the amino acid sequence of Plk1-(1–98) identified one cluster of basic amino acids (^{48}RSRRRYVRGR^{57}), suggesting that this basic cluster acts as a nuclear localization signal. We then tested the interaction between p53 and each of these Plk1 deletion mutants. COS7 cells were transfected with the expression plasmid encoding Plk1-(1–401), Plk1-(1–329), or Plk1-(1–98), and co-immunoprecipitation experiments were performed to determine the interaction. We found that Plk1-(1–401) and Plk1-(1–329) retained the ability to bind to p53, whereas Plk1-(1–98) did not (Fig. 5*C*). These results indicate that the amino acid sequence comprising residues 99 to 329 of Plk1 contains the p53-binding domain.

Plk1 Inhibits the p53-mediated Transcriptional Activation—To determine whether Plk1 could affect the transcriptional activity of p53, H1299 cells were transiently co-transfected with a constant amount of the expression plasmid encoding p53 together with the p53-responsive $p21^{WAF1}$, *MDM2*, or *BAX*-luciferase reporter constructs in the presence or absence of increasing amounts of the expression plasmid for FLAG-Plk1. Under our experimental conditions, ectopically expressed p53 successfully activated the transcription of each of those p53-responsive reporters as compared with the empty plasmid controls, but Plk1 alone had no effect on luciferase activity (Fig. 6). Expression of FLAG-Plk1 greatly reduced the ability of p53 to increase the $p21^{WAF1}$-, *MDM2*-, and *BAX*-luciferase activities in a dose-dependent manner (Fig. 6, *A–C*). In addition, Plk1-(1–98), which lacks an ability to interact with p53, did not affect the p53 transcriptional activity toward the $p21^{WAF1}$, *MDM2*, and *BAX* promoters (data not shown). To confirm the inhibitory role of Plk1 in the p53-mediated transactivation, we assayed H1299 cell transfectants for induction of the endoge-